Journal of Cosmology and
Astroparticle Physics

SISSA

PAPER

Testing the equivalence principle on cosmological scales using the odd multipoles of galaxy cross-power spectrum and bispectrum

To cite this article: Obinna Umeh *et al* JCAP08(2021)049

Journal of Cosmology and Astroparticle Physics
An IOP and SISSA journal

Testing the equivalence principle on cosmological scales using the odd multipoles of galaxy cross-power spectrum and bispectrum

Obinna Umeh,* Kazuya Koyama and Robert Crittenden

Institute of Cosmology & Gravitation, University of Portsmouth, Portsmouth PO1 3FX, United Kingdom

E-mail: obinna.umeh@port.ac.uk, kazuya.koyama@port.ac.uk, robert.crittenden@port.ac.uk

Received December 1, 2020
Revised July 5, 2021
Accepted July 30, 2021
Published August 23, 2021

Abstract. One of the cornerstones of general relativity is the equivalence principle. However, the validity of the equivalence principle has only been established on solar system scales for standard matter fields; this result cannot be assumed to hold for the non-standard matter fields that dominate the gravitational dynamics on cosmological scales. Here we show how the equivalence principle may be tested on cosmological scales for non-standard matter fields using the odd multipoles of the galaxy cross-power spectrum and bispectrum. This test makes use of the imprint on the galaxy cross-power spectrum and bispectrum by the parity-violating general relativistic deformations of the past-light cone, and assumes that galaxies can be treated as test particles that are made of baryons and cold dark matter. This assumption leads to a non-zero galaxy-baryon relative velocity if the equivalence principle does not hold between baryons and dark matter. We show that the relative velocity can be constrained to be less than 28% of the galaxy velocity using the cross-power spectrum of the HI intensity mapping/Hα galaxy survey and the bispectrum of the Hα galaxy survey.

Keywords: gravity, modified gravity, cosmological parameters from LSS

ArXiv ePrint: 2011.05876

*Corresponding author.

https://doi.org/10.1088/1475-7516/2021/08/049

JCAP08(2021)049

Contents

1 Introduction

One of the foundational pillars of general relativity is Einstein's equivalence principle. The equivalence principle says that all bodies fall at the same rate in a local gravitational field independently of their material make-up. Finding violations of the equivalence principle could provide clues to the nature of gravitational theories beyond general relativity [1]. In cosmology, it could unveil the fundamental nature of dark matter and dark energy as well as the possible gravitational interaction between them [2].

There have been various tests of the equivalence principle, starting with terrestrial studies of objects with different compositions freely falling in a vacuum [3, 4]. MICROSCOPE [5] tests the equivalence principle by comparing the acceleration of two masses (one made of platinum alloy and the other titanium alloy) that follow the same orbit around Earth for a long period of time.[1] The equivalence principle has so far been confirmed by all these tests; however, these tests have been carried out on the solar system scale with test particles whose composition we understand.[2] Therefore, these results cannot easily be extrapolated to cosmology [10], where the unknown nature of cold dark matter, dark energy, gravity and backreaction is crucial to the evolution of the universe on large scales [11, 12]. It is not clear whether the equivalence principle holds for these types of matter or gravity on large scales.

[1] There are other tests of the equivalence principle that rely on the extra time delay that the gravitational field could cause to a propagating photon [6, 7] or gravitational waves [8]. These tests confirm the equivalence principle on inter-galactic scales but the level of precision of the measurement is still below the requirement for precision cosmology.

[2] There are constraints on an exotic coupling between ordinary and dark matter by laboratory tests of the weak equivalence when analysed as a test of the uniformity of free fall towards the centre of the Galaxy [9].

JCAP08(2021)049

Recently a method of testing the equivalence principle on cosmological scales was proposed, based on the understanding that the validity of the consistency relation between the squeezed limit of correlation functions of large scale structures is a consequence of the equivalence principle [13, 14]. This connection implies that any physical process that violates the equivalence principle will lead to a breakdown of the consistency relation. Although this approach depends only on the squeezed configuration of the correlation function of galaxies, an analysis including all possible shapes of the bispectrum leads to an impressive constraint on the strength of the coupling of the galaxy velocity to the fifth force. In this paper, we describe how the number count of sources may be used to test the equivalence principle on cosmological scales by looking at the odd multipole moments of the correlation functions of the large scale structures.

The number of galaxies we observe today within a redshift slice and solid angle is impacted by a number of physical effects due to the inhomogeneities along the line of sight. At leading order, the galaxy position is displaced by the peculiar velocity of the source. The effect of the displacement on the number count fluctuations is dominated by the redshift space distortion known as the Kaiser effect [15]. The Kaiser effect provides an avenue to test alternative theories of gravity on large scales through the measurement of the growth rate of structures [16]. The Kaiser effect induces only even multipoles of the galaxy power spectrum and bispectrum. The next-to-leading order effect on galaxy clustering is the Doppler effect, which introduces a shift in galaxy redshift whose imprint depends on the relative position of the galaxy with respect to the line of sight [17–20]. The Doppler effect induces only odd multipoles of the galaxy cross-power spectrum and bispectrum [21]. We utilise these distinct imprints of the Doppler effect on the galaxy cross-power spectrum and bispectrum to develop a consistent framework for testing the equivalence principle on cosmological scales.

The dipole of the galaxy cross-power spectrum has been detected in the CMASS sample of the BOSS survey [22] and is seen in N-body simulations [23] by considering haloes selected based on different mass criteria. In [24], Bonvin and Fleury proposed to use the dipole in the galaxy cross-power spectrum to test the equivalence principle. The approach taken in [24] differs substantially from the formalism we discuss here. In particular, they proposed a parametrisation of a large class of modified Euler equation for dark matter and studied how the galaxy cross-power spectrum could constrain the parameters. They also assumed that the peculiar velocities of galaxies are determined only by dark matter, and neglected the effect of baryons.

In this paper, in addition to the dipole of the galaxy cross-power spectrum, we include the contribution from the dipole and octupole moments of the galaxy bispectrum. We also parametrise the odd multipoles differently from ref. [24]. We do not neglect the effects of baryons, rather we assume that galaxies can be treated as test particles that are made of cold dark matter and baryons, and baryons satisfy the standard Euler equation. This allows us to directly parametrise the relative velocity between galaxies and baryons rather than parametrising the modified Euler equation for dark matter. The parametrisation we propose makes apparent the baryon-dark matter relative velocity that we are interested in. The parametrisation is independent of theories of gravity but we discuss in detail a limit of this parametrisation that applies to a class of modified theories of gravity where the scale dependence of the fifth force is negligible. We show that a Stage IV HI intensity mapping and the Hα emission line galaxy survey, which overlaps in about 0.38 fraction of the sky, will be able to constrain the relative velocity of baryons and galaxies to be less than 28% of the galaxy velocity via the galaxy cross-power spectrum and the bispectrum of the Hα galaxy survey.

JCAP08(2021)049

The rest of the paper is structured as follows: in section 2 we introduce the full non-perturbative expression for the number count of galaxies on arbitrary spacetime: we perturb it on an FLRW background in subsection 2.1, and discuss the equivalence principle for baryons in subsection 2.2. We adopt the standard Eulerian bias model for the galaxy density field in section 3, discussing the decomposition of the galaxy cross-power spectrum and bispectrum in multipoles in section 3.1. We derive covariance matrix and describe the Fisher forecast analysis technique in section 4 and conclude in section 5. An example of how baryon-dark matter relative velocity could be sourced by an interaction in the dark sector is discussed in appendix A.

Notations. We neglect the effect of radiation and the anisotropic stress tensor, which is sufficiently accurate at $z \leq 20$. We adopt the standard normalisation for the Taylor series expansion of any quantity X: $X = \bar{X} + X^{(1)} + X^{(2)}/2$ where $\bar{X}$ denotes the FLRW background component, $X^{(1)}$ and $X^{(2)}$ are first and second order perturbations, respectively. We decompose each perturbed quantity at order n into two parts $X^{(n)} = X^{(n)}_{\rm N} + X^{(n)}_{\rm GR}$, where $X^{(n)}_{\rm N}$ denotes the Newtonian approximation of $X^{(n)}$, while $X^{(n)}_{\rm GR}$ denotes the general relativistic corrections. We consider the limit where only the Doppler effect dominates in $X^{(n)}_{\rm GR}$ and therefore set $X^{(n)}_{\rm GR} = X^{(n)}_{\rm D}$. For the fiducial cosmological parameters we adopt the Planck 2018 best-fit values [10]: Hubble parameter, $h = 0.674$, baryon density parameter, $\Omega_b = 0.0493$, dark matter density parameter, $\Omega_{\rm cdm} = 0.264$, spectral index, $n_s = 0.9608$, and the amplitude of the primordial perturbation, $A_s = 2.198 \times 10^9$.

2 Galaxy number counts

The number of galaxies seen by an observer at o with a flux greater than F per redshift bin and per solid angle is given by [25–27]:

$$\frac{{\rm dN}^{\rm obs}(z, \hat{\mathbf{n}}, F)}{{\rm dz}\, {\rm d}\Omega_o} = \mathcal{N}_g(z, \hat{\mathbf{n}}, F)\, d_A^2(z, \hat{\mathbf{n}})\, [k_\mu u^\mu]_o \left|\frac{d\lambda}{dz}\right|, \tag{2.1}$$

where z is the observed redshift of the source, λ is the affine parameter (comoving distance) to the source, $\hat{\mathbf{n}}$ is the line of sight direction to the source, u^μ is the 4-velocity of the source galaxy, k^μ is the photon tangent vector, d_A is the angular diameter distance to the source and $\mathcal{N}_g$ is the flux-limited proper number density of galaxy

$$\mathcal{N}_g(z, \hat{\mathbf{n}}, F) = \int_{\ln L(F)}^{\infty} d\ln L\; n_g(z, \hat{\mathbf{n}},] \ln L)\,. \tag{2.2}$$

Here n_g is the proper number density of sources. The luminosity of the source is related to its flux by $L = 4\pi F d_L^2 = 4\pi F (1+z)^4 d_A^2$.

The expansion of equation (2.1) up to second order in perturbation theory has been done by several authors [28–30]. However, they all assumed that the motion of galaxies traces that of dark matter and that dark matter obeys the equivalence principle. This is the key assumption we relax here.

We consider metric perturbations in Poisson gauge on a background FLRW spacetime:

$$ds^2 = a^2 \left(-(1+2\Phi)\, d\eta^2 + (1-2\Psi)\, \delta_{ij} dx^i dx^j \right), \tag{2.3}$$

where Φ and Ψ are the metric perturbations, "a" is the scale factor of the background FLRW spacetime, η is the conformal time. We neglect the vector and tensor perturbation at first and

JCAP08(2021)049

second order, because they are sub-dominant in this gauge [31]. For a given fluid component I, the perturbation of the temporal and spatial components of its 4-velocity is given by

$$u_I^0 = 1 - \Phi^{(1)} + \frac{1}{2}\left[3[\Phi^{(1)}]^2 - \Phi^{(2)} + \partial_i v_I^{(1)} \partial^i v_I^{(1)}\right], \tag{2.4}$$

$$u_I^i = \partial^i v_I^{(1)} + \frac{1}{2}\partial^i v_I^{(2)}, \tag{2.5}$$

where v_I is the I-th peculiar velocity potential. We shall see later how the peculiar velocity potential of each of the fluid components is related to Φ via the generalised Euler equation.

2.1 Gravity theory independent number count in the weak-field limit

In the weak-field limit, we neglect integrated terms such as weak gravitational lensing, the integrated Sachs-Wolfe effect, the time-delay effect, etc. The contributions from such terms are expected to be sub-dominant for thin redshift bins, although they could be important when cross-correlations between widely separated redshift bins are considered [32, 33]. We shall introduce the basic notations here and refer the reader to [28, 34] for details on the derivation. Expanding equation (2.2) in perturbation theory leads to

$$\mathcal{N}_g(z, \hat{\mathbf{n}}, \bar{L}) = \bar{\mathcal{N}}_g(z, \bar{L})\left[1 + \delta_g + b_e \Delta_z + \mathcal{Q}\Delta_{d_L} + \frac{\partial \delta_g}{\partial \ln \bar{L}}\Delta_{d_L}\right], \tag{2.6}$$

where we have introduced the following short-hand notations for simplicity: the perturbation in the galaxy number density $\delta_g \equiv \delta_g(z, \hat{\mathbf{n}}, \bar{L})$, the magnification bias parameter $\mathcal{Q} \equiv \mathcal{Q}(z, \bar{L})$, which is related to the slope of the luminosity function s according to $\mathcal{Q} = 5s/2$, the evolution bias parameter $b_e \equiv b_e(z, \bar{L})$, the redshift perturbation $\Delta_z \equiv \Delta_z(z, \hat{\mathbf{n}})$ and the perturbation of the luminosity distance $\Delta_{d_L} \equiv \Delta_{d_L}(z, \hat{\mathbf{n}})$. Putting all these in equation (2.1) and expanding everything up to second order leads to

$$\frac{\mathrm{dN^{obs}}(z, \hat{\mathbf{n}}, F)}{\mathrm{dz\, d\Omega_o}} = \frac{\mathrm{d\bar{N}}(z, F)}{\mathrm{dz\, d\Omega_o}}\left[1 + \Delta^{(1)}_{\mathrm{N^{obs}}}(z, \hat{\mathbf{n}}, F) + \frac{1}{2}\Delta^{(2)}_{\mathrm{N^{obs}}}(z, \hat{\mathbf{n}}, F)\right], \tag{2.7}$$

where $\mathrm{d\bar{N}}(z, F)/\mathrm{dz\, d\Omega_o}$ is the mean number count per redshift bin per solid angle and $\Delta_{\mathrm{N^{obs}}}$ is fluctuation. We can write $\Delta_{\mathrm{N^{obs}}} = \Delta_{\mathrm{N}} + \Delta_{\mathrm{D}}$, where at linear order

$$\Delta^{(1)}_{\mathrm{N}} = \delta_g^{(1)} - \frac{1}{\mathcal{H}}\partial_\parallel^2 v_g{}^{(1)}, \tag{2.8}$$

$$\Delta^{(1)}_{\mathrm{D}} = \partial_\parallel v_g{}^{(1)} + \frac{1}{\mathcal{H}}\left(\partial_\parallel v_g{}^{(1)\prime} + \partial_\parallel \Phi^{(1)}\right) + \left[b_e - 2\mathcal{Q} - \frac{2\,(1-\mathcal{Q})}{\chi\mathcal{H}} - \frac{\mathcal{H}'}{\mathcal{H}^2}\right]\partial_\parallel v_g{}^{(1)}, \tag{2.9}$$

where $\partial_\parallel^2 v_g{}^{(1)} = n^i n^j \partial_i \partial_j v_g{}^{(1)}$. The equation (2.8) is the well-known Kaiser limit [15] of the number count fluctuations, which constitutes what we call the Newtonian approximation $\Delta^{(1)}_{\mathrm{N}}$. Equation (2.9) contains the leading order contribution to the large-scale general relativistic effects; $\Delta^{(1)}_{\mathrm{D}}$ is dominated by the Doppler effects [35]. Equation (2.9) is independent of any

JCAP08(2021)049

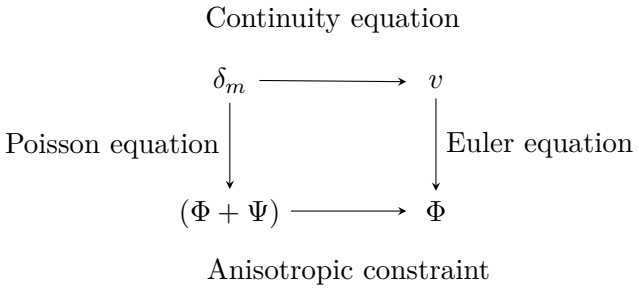

Figure 1. Scalar perturbations in Poisson-gauge have four independent degrees of freedom: two from the matter sector, δ_m(matter density), v (peculiar velocity) and two from the metric sector, Φ (gravitational potential), and Ψ (curvature perturbation). Large scale structure survey measures δ_m via clustering of biased tracers, v via the redshift space distribution, Φ via the Doppler effect and $\Phi + \Psi$ via weak gravitational lensing.

theory of gravity. At second order, we find

$$\begin{aligned}\Delta_{\rm N}^{(2)} &= \delta_g^{(2)} - \frac{1}{\mathcal{H}}\partial_\parallel^2 v_g{}^{(2)} - \frac{2}{\mathcal{H}}\left[\delta_g^{(1)}\partial_\parallel^2 v_g{}^{(1)} + \partial_\parallel v_g{}^{(1)}\partial_\parallel \delta_g^{(1)}\right] + \frac{2}{\mathcal{H}^2}\left[\left(\partial_\parallel^2 v_g{}^{(1)}\right)^2\right. \\ &\quad \left. + \partial_\parallel v_g{}^{(1)}\partial_\parallel^3 v_g^{(1)}\right], \qquad (2.10)\\ \Delta_{\rm D}^{(2)} &= \left[1 + b_e - 2\mathcal{Q} - \frac{2\,(1-\mathcal{Q})}{\chi\mathcal{H}} - \frac{\mathcal{H}'}{\mathcal{H}^2}\right]\partial_\parallel v_g{}^{(2)} + \frac{1}{\mathcal{H}}\left(\partial_\parallel v_g{}^{(2)\prime} + \partial_\parallel \Phi^{(2)}\right) \\ &\quad + \frac{2}{\mathcal{H}}\left[\delta_g^{(1)} - \frac{2}{\mathcal{H}}\partial_\parallel^2 v_g{}^{(1)}\right]\left[\partial_\parallel v_g{}^{(1)\prime} + \partial_\parallel \Phi^{(1)}\right] + \frac{2}{\mathcal{H}}\Phi^{(1)}\left[\partial_\parallel \delta_g^{(1)} - \frac{1}{\mathcal{H}}\partial_\parallel^3 v_g{}^{(1)}\right] \\ &\quad + 4\partial_\parallel v_g{}^{(1)}\left(1 - \frac{1}{\chi\mathcal{H}}\right)\frac{\partial\delta_g^{(1)}}{\partial \ln L} + 2\partial_\parallel v_g{}^{(1)}\delta_g^{(1)}\left[1 + b_e - 2\mathcal{Q} - \frac{2\,(1-\mathcal{Q})}{\chi\mathcal{H}} - \frac{\mathcal{H}'}{\mathcal{H}^2}\right] \\ &\quad + \frac{2}{\mathcal{H}}\partial_\parallel v_g{}^{(1)}\left[\delta_g^{(1)\prime} - \frac{2}{\mathcal{H}}\partial_\parallel^2 v_g{}^{(1)\prime} - \frac{1}{\mathcal{H}}\partial_\parallel^2 \Phi^{(1)}\right] - \frac{2}{\mathcal{H}}\nabla_{\perp i} v_g{}^{(1)}\nabla_\perp^i \partial_\parallel v_g{}^{(1)} \\ &\quad + \frac{2}{\mathcal{H}}\partial_\parallel v_g{}^{(1)}\partial_\parallel^2 v_g{}^{(1)}\left[-2 - 2b_e + 4\mathcal{Q} + \frac{4\,(1-\mathcal{Q})}{\chi\mathcal{H}} + 3\frac{\mathcal{H}'}{\mathcal{H}^2}\right]. \qquad (2.11)\end{aligned}$$

Furthermore, equation (2.9) contains the gradient of the gravitational potential, while equation (2.11) contains both the gravitational potential and the gradient of the gravitational potential. In order to express them in terms of the Doppler peculiar velocity, the Euler equation is required. See figure 1 for the relationships between scalar perturbation variables.

The classification of the second order terms into Newtonian and Doppler terms is a little more complicated. However, we found that the most consistent way to classify all the terms is to think of the density term and the velocity term as a function of the gravitational potential through the Poisson equation (in sub-horizon limit) and the baryon Euler equation, respectively. Within this scheme, the quadratic second-order Newtonian terms will be proportional to four spatial derivatives of two gravitational potentials. How the derivatives act on the gravitational potentials does not matter. Similarly, the quadratic second-order Doppler terms in equation (2.11) contain only terms with three spatial derivatives of the two gravitational potentials. Again, how the derivatives act on the gravitational potentials does not matter, what is important is the number of spatial derivatives.

JCAP08(2021)049

Galaxies are made of baryons and dark matter. In the standard case, both baryons and dark matter are assumed to follow the same geodesic equation

$$\partial^i {v_m}^{(1)\prime} + \mathcal{H}\partial^i {v_m}^{(1)} + \partial^i \Phi^{(1)} = 0\,. \tag{2.12}$$

If the galaxy velocity exactly coincides with the matter velocity $v_g = v_m$, we can use equation (2.12) and its second order equivalent to relate Φ to v_g, and the result is the well-known expression for the general relativistic number count fluctuation given in [26, 36, 37] at linear order and in [28–30, 38] at second order.

2.2 Beyond the standard case: equivalence principle for baryons only

We assume that only the baryon motion is geodesic, hence they satisfy the standard Euler equation. At the linear order, the Euler equation for baryons is given by

$$\partial^i {v_b}^{(1)\prime} + \mathcal{H}\partial^i {v_b}^{(1)} + \partial^i \Phi^{(1)} = 0\,, \tag{2.13}$$

where $v_b^{(1)}$ is the linear baryon peculiar velocity potential. Using equation (2.13) in equation (2.9) to relate the gravitational potential to the baryon velocity. we find

$$\begin{aligned}\Delta_{\rm D}^{(1)} &= \partial_\parallel {v_g}^{(1)} - \partial_\parallel {v_b}^{(1)} \\ &\quad + \frac{1}{\mathcal{H}}\left(\partial_\parallel {v_g}^{(1)\prime} - \partial_\parallel {v_b}^{(1)\prime}\right) + \left[b_e - 2\mathcal{Q} - \frac{2\,(1-\mathcal{Q})}{\chi\mathcal{H}} - \frac{\mathcal{H}'}{\mathcal{H}^2}\right]\partial_\parallel {v_g}^{(1)}\,.\end{aligned} \tag{2.14}$$

Similarly, the Euler equation for baryons at second order in the weak field limit is given by

$$\partial_i v_b^{(2)\prime} + \mathcal{H}\partial_i v_b^{(2)} + \partial_i \Phi^{(2)} + 2\partial_i\partial_j v_b^{(1)}\partial^j v_b^{(1)} + \mathcal{O}(\Phi^{(1)}\partial\Phi) = 0\,. \tag{2.15}$$

Using equations (2.13) and (2.15), we can relate $\Phi^{(1)}$ to $v_b^{(1)}$ and $\Phi^{(2)}$ to $v_b^{(2)}$ in equation (2.11). After straight-forward but lengthy algebra we find

$$\begin{aligned}\Delta_{\rm D}^{(2)} &= \left[b_e - 2\mathcal{Q} - \frac{2\,(1-\mathcal{Q})}{\chi\mathcal{H}} - \frac{\mathcal{H}'}{\mathcal{H}^2}\right]\partial_\parallel {v_g}^{(2)} + (\partial_\parallel {v_g}^{(2)} - \partial_i v_b^{(2)}) + \frac{1}{\mathcal{H}}\left(\partial_\parallel {v_g}^{(2)\prime} - \partial_i v_b^{(2)\prime}\right) \\ &\quad - \frac{2}{\mathcal{H}}\partial_\parallel\partial_j v_b^{(1)}\partial^j v_b^{(1)} + \frac{2}{\mathcal{H}}\left[\delta_g^{(1)} - \frac{2}{\mathcal{H}}\partial_\parallel^2 {v_g}^{(1)}\right]\left[\partial_\parallel {v_g}^{(1)\prime} - \partial_\parallel v_b^{(1)\prime} - \mathcal{H}\partial_\parallel v_b^{(1)}\right] \\ &\quad - \frac{2}{\mathcal{H}}\left[v_b^{(1)\prime} + \mathcal{H}v_b^{(1)}\right]\left[\partial_\parallel\delta_g^{(1)} - \frac{1}{\mathcal{H}}\partial_\parallel^3 {v_g}^{(1)}\right] \\ &\quad + 4\partial_\parallel {v_g}^{(1)}\left(1 - \frac{1}{\chi\mathcal{H}}\right)\frac{\partial\delta_g^{(1)}}{\partial\ln L} + 2\partial_\parallel {v_g}^{(1)}\delta_g^{(1)}\left[1 + b_e - 2\mathcal{Q} - \frac{2\,(1-\mathcal{Q})}{\chi\mathcal{H}} - \frac{\mathcal{H}'}{\mathcal{H}^2}\right] \\ &\quad + \frac{2}{\mathcal{H}}\partial_\parallel {v_g}^{(1)}\left[\delta_g^{(1)\prime} - \frac{2}{\mathcal{H}}\partial_\parallel^2 {v_g}^{(1)\prime} + \frac{1}{\mathcal{H}}\partial_\parallel^2 v_b^{(1)\prime} + \partial_\parallel^2 v_b^{(1)}\right] - \frac{2}{\mathcal{H}}\nabla_{\perp i}{v_g}^{(1)}\nabla_\perp^i\partial_\parallel {v_g}^{(1)} \\ &\quad + \frac{2}{\mathcal{H}}\partial_\parallel {v_g}^{(1)}\partial_\parallel^2 {v_g}^{(1)}\left[-2 - 2b_e + 4\mathcal{Q} + \frac{4\,(1-\mathcal{Q})}{\chi\mathcal{H}} + 3\frac{\mathcal{H}'}{\mathcal{H}^2}\right]\,.\end{aligned} \tag{2.16}$$

We parametrise the relative velocity between galaxy peculiar velocity v_g and baryon peculiar velocity v_b as

$$v_g^{(1)} - v_b^{(1)} = v_{gb}^{(1)} \equiv \Upsilon_1 v_g^{(1)}, \quad v_g^{(2)} - v_b^{(2)} = v_{gb}^{(2)} \equiv \Upsilon_2 v_g^{(2)}\,. \tag{2.17}$$

We have introduced two spacetime dependent parameters $\Upsilon_1 = \Upsilon_1(\eta, \boldsymbol{x})$ and $\Upsilon_2 = \Upsilon_2(\eta, \boldsymbol{x})$ which modulate the linear order galaxy-baryon relative velocity, $v_{gb}^{(1)}$, and the second order

JCAP08(2021)049

galaxy-baryon relative velocity, $v^{(2)}_{gb}$, respectively. This might appear to be introducing too many parameters to describe the same physical effect; however, this is not the case especially for modified gravity theories where the second order dark matter density field and peculiar velocity satisfy non-linear second order differential equations, thus its evolution could be significantly different from the linear order expression as shown in appendix A. We parametrise the derivative with respect to conformal time as

$$v_g{}^{(1)\prime} - v_b{}^{(1)\prime} = v^{(1)\prime}_{gb} = \beta_1 v^{(1)\prime}_g, \quad v_g{}^{(2)\prime} - v_b{}^{(2)\prime} = v^{(2)\prime}_{gb} = \beta_2 v^{(2)\prime}_g . \tag{2.18}$$

For simplicity, we assume that Υ_1 and Υ_2 are a smooth and well-behaved functions of the conformal time only. In this limit, $\{\beta_1, \beta_2\}$ may be expressed in terms of $\{\Upsilon_1, \Upsilon_2\}$;

$$\beta_1 = \frac{\Upsilon_1'}{\bar{X}_{g1}} + \Upsilon_1 , \qquad \beta_2 = \frac{\Upsilon_2'}{\bar{X}_{g2}} + \Upsilon_2 , \tag{2.19}$$

where $\bar{X}_{g1} \equiv v_g{}^{(1)\prime}/v_g{}^{(1)}$ and $\bar{X}_{g2} \equiv v_g{}^{(2)\prime}/v_g{}^{(2)}$. With these, we can express the galaxy number count in terms of δ_g and v_g only. The only assumptions we have made so far is that baryons obey the standard Euler equation (the equivalence principle) and that the galaxy-baryon relative velocity is a function of the observed galaxy velocity with a time-dependent amplitude only. We note that scale dependence may arise from the mass of the scalar field that mediates the fifth force. Scale-dependent growth will be better constrained by the even multipole moments of the power spectrum and bispectrum. In the rest of the paper, we assume that scale dependence can be ignored on scales relevant to our analysis.

3 Model independent constraint on the relative velocity

We assume that the galaxy density is well described in terms of the total matter density δ_m and the scalar invariant of the tidal field tensor $\mathcal{S}^2$ according to

$$\delta_{\rm g} = b_1 \delta^{(1)}_m + \frac{1}{2}\left[b_1 \delta^{(2)}_m + b_2 (\delta^{(1)}_{\rm m})^2 + b_{s^2} \mathcal{S}^2 \right], \tag{3.1}$$

where b_1, b_2 and $b_{\mathcal{S}^2}$ are linear, non-linear and tidal bias, respectively. In principle, the existence of a non-vanishing v_{gb} could contribute extra terms to the galaxy bias formula given in equation (3.1). (For the case of v_{gb} sourced during the photon-Baryon decoupling, preliminary studies have indicated that the effect of such terms is negligible for a Stage IV large scale structure survey [39, 40].) For our purposes, we can ignore such terms because the galaxy density will be directly constrained by the even multipoles of the N-point correlation function [40, 41]. Similarly, we neglect the general relativistic corrections to equation (3.1) since they become important near Hubble horizon scales [42], whose consideration is beyond the scope of this work.

The matter density at first order is given by $\delta^{(1)}_m(\boldsymbol{k}, \eta) = D_m(\eta)\delta^{(1)}_O(\boldsymbol{k})$, where D_m is the growth of the matter density field (for simplicity, we assume that it is a function of the conformal time only.), $\delta_O(\boldsymbol{k})$ is related to the initial density field via the transfer function $T(k)$: $\delta_O(\boldsymbol{k}) = \delta_{\rm ini}(\boldsymbol{k})T(k)$. At second order the matter density and tidal tensor invariant are given by

$$\delta^{(2)}_m(\boldsymbol{k}, \eta) = \int \frac{d^3k_1}{(2\pi)^3}\frac{d^3k_2}{(2\pi)^3} F_2(\boldsymbol{k}_1, \boldsymbol{k}_2)\delta_m(\boldsymbol{k}_1, \eta)\delta_m(\boldsymbol{k}_2, \eta)(2\pi)^3\delta^{(3)}\left(\boldsymbol{k} - \boldsymbol{k}_1 - \boldsymbol{k}_2\right) , \tag{3.2}$$

$$\mathcal{S}^2(\boldsymbol{k}, \eta) = \int \frac{d^3k_1}{(2\pi)^3}\frac{d^3k_2}{(2\pi)^3} S_2(\boldsymbol{k}_1, \boldsymbol{k}_2)\delta_m(\boldsymbol{k}_1, \eta)\delta_m(\boldsymbol{k}_2, \eta)(2\pi)^3\delta^{(3)}\left(\boldsymbol{k} - \boldsymbol{k}_1 - \boldsymbol{k}_2\right) , \tag{3.3}$$

JCAP08(2021)049

where F_2 and S_2 are the Fourier space kernels of the matter density field and the scalar invariant of the tidal field tensor, respectively. Similarly, we model the galaxy velocity in terms of the matter density field as follows

$$v_g^{(1)}(\boldsymbol{k},\eta) = \frac{\mathcal{H}}{k^2} f_g \delta_m^{(1)}(\boldsymbol{k},\eta)\,, \tag{3.4}$$

$$v_g^{(2)}(\boldsymbol{k},\eta) = \frac{\mathcal{H} f_g}{k^2} \int \frac{d^3k_1}{(2\pi)^3}\frac{d^3k_2}{(2\pi)^3} G_2(\boldsymbol{k}_1,\boldsymbol{k}_2)\delta_m(\boldsymbol{k}_1,\eta)\delta_m(\boldsymbol{k}_2,\eta)\delta^{(3)}\left(\boldsymbol{k}-\boldsymbol{k}_1-\boldsymbol{k}_2\right)\,, \tag{3.5}$$

where f_g is the growth rate of structure (again f_g is a function of the conformal time only), and G_2 and S_2 is the kernel of the velocity potential. We assume that these kernels are well described by

$$F_2(\boldsymbol{k}_1,\boldsymbol{k}_2) = \frac{10}{7} + \frac{\boldsymbol{k}_1\cdot\boldsymbol{k}_2}{k_1k_2}\left(\frac{k_1}{k_2}+\frac{k_2}{k_1}\right) + \frac{4}{7}\left(\frac{\boldsymbol{k}_1\cdot\boldsymbol{k}_2}{k_1k_2}\right)^2\,, \tag{3.6}$$

$$G_2(\boldsymbol{k}_1,\boldsymbol{k}_2) = \frac{6}{7} + \frac{\boldsymbol{k}_1\cdot\boldsymbol{k}_2}{k_1k_2}\left(\frac{k_1}{k_2}+\frac{k_2}{k_1}\right) + \frac{8}{7}\left(\frac{\boldsymbol{k}_1\cdot\boldsymbol{k}_2}{k_1k_2}\right)^2\,, \tag{3.7}$$

$$S_2(\boldsymbol{k}_1,\boldsymbol{k}_2) = \frac{(\boldsymbol{k}_1\cdot\boldsymbol{k}_2)^2}{(k_1k_2)^2} - \frac{1}{3}\,. \tag{3.8}$$

Given equations (3.4) and (3.5), the conformal time derivative of v_g becomes

$$v^{(1)\prime}_g(\boldsymbol{k},\eta) = \frac{\mathcal{H}^2 f_g}{k^2} X_{g1}\delta_m(\boldsymbol{k},\eta)\,, \tag{3.9}$$

$$v_g^{(2)\prime}(\boldsymbol{k},\eta) = \frac{\mathcal{H}^2 f_g X_{g2}}{k^2} \int \frac{d^3k_1}{(2\pi)^3}\frac{d^3k_2}{(2\pi)^3} G_2(\boldsymbol{k}_1,\boldsymbol{k}_2)\delta_m(\boldsymbol{k}_1,\eta)\delta_m(\boldsymbol{k}_2,\eta)\delta^{(3)}\left(\boldsymbol{k}-\boldsymbol{k}_1-\boldsymbol{k}_2\right)\,. \tag{3.10}$$

Note that $\bar{X}_{g1} = \mathcal{H}X_{g1}$ and $\bar{X}_{g2} = \mathcal{H}X_{g2}$, where

$$X_{g1} = \frac{f_g{}'}{\mathcal{H}f_g} + f_g + \frac{\mathcal{H}'}{\mathcal{H}^2}\,, \qquad X_{g2} = \frac{f_g{}'}{\mathcal{H}f_g} + 2f_g + \frac{\mathcal{H}'}{\mathcal{H}^2}\,. \tag{3.11}$$

We will assume that δ_g and v_g are precisely determined by the even multipoles. With these tools we expand equations (2.8) and (2.10) in Fourier space. In the Newtonian limit, the Fourier space kernel becomes [43]

$$\mathcal{K}_{\rm N}^{(1)}(k_1) = b_1 + f_g\mu_1^2\,, \tag{3.12}$$

$$\begin{aligned}\mathcal{K}_{\rm N}^{(2)}(\boldsymbol{k}_1,\boldsymbol{k}_2,\boldsymbol{k}_3) = {}& b_2 + b_1F_2(\boldsymbol{k}_1,\boldsymbol{k}_2) + b_{s^2}S_2(\boldsymbol{k}_1,\boldsymbol{k}_2) + f_g\,G_2(\boldsymbol{k}_1,\boldsymbol{k}_2)\mu_3^2 \\ & + b_1f_g\left[\left(\mu_1^2+\mu_2^2\right) + \mu_1\mu_2\left(\frac{k_1}{k_2}+\frac{k_2}{k_1}\right)\right] + f_g^2\left[2\mu_1^2\mu_2^2 + \mu_1\mu_2\left(\mu_1^2\frac{k_1}{k_2}+\mu_2^2\frac{k_2}{k_1}\right)\right]\,,\end{aligned} \tag{3.13}$$

where $\mu_m = \hat{\boldsymbol{k}}_m\cdot\hat{\mathbf{n}} = \boldsymbol{k}_m\cdot\hat{\mathbf{n}}/k_m$ with $m\in\{1,2,3\}$. The Fourier space kernels for the Doppler

JCAP08(2021)049

part (i.e. equations (2.14) and (2.16)) become

$$\mathcal{K}_{\rm D}^{(1)}(k_1) = \mathcal{H}\frac{f_g B_1}{k}\mu_1\,, \tag{3.14}$$

$$\begin{aligned}\mathcal{K}_{\rm D}^{(2)}(\boldsymbol{k}_1,\boldsymbol{k}_2,\boldsymbol{k}_3) = \mathcal{H}\Bigg\{ &\frac{f_g\mu_3}{k_3}A_0 G_2(\boldsymbol{k}_1,\boldsymbol{k}_2) - b_1 f_g A_1\left(\frac{\mu_1 k_2^3+\mu_1 k_1^3}{k_1^2k_2^2}\right) + f_g A_2\left(\frac{\mu_1}{k_1}+\frac{\mu_2}{k_2}\right)\\ &+ f_g^2\Bigg[A_4\left(\boldsymbol{k}_1\cdot\boldsymbol{k}_2\right)\left(\frac{\mu_1 k_1+\mu_2 k_2}{k_1^2k_2^2}\right) - (1+A_3)\left(\frac{\mu_1\mu_2^2 k_1 k_2^2+\mu_2\mu_1^2 k_2 k_1^2}{k_1^2k_2^2}\right)\\ &- A_1\left(\frac{\mu_2^3k_2^3+\mu_1^3k_1^3}{k_1^2k_2^2}\right)\Bigg]\Bigg\}\,,\end{aligned} \tag{3.15}$$

where B_1, A_0, A_1, A_2, A_3 and A_4 are redshift dependent terms

$$B_1 = \Upsilon_1 + \beta_1 X_{g1} + b_e - 2\mathcal{Q} - \frac{2\,(1-\mathcal{Q})}{\chi\mathcal{H}} - \frac{\mathcal{H}'}{\mathcal{H}^2}\,, \tag{3.16}$$

$$A_0 = \Upsilon_2 + \beta_2 X_{g2} + b_e - 2\mathcal{Q} - \frac{2\,(1-\mathcal{Q})}{\chi\mathcal{H}} - \frac{\mathcal{H}'}{\mathcal{H}^2}\,, \tag{3.17}$$

$$A_1 = (1-\beta_1)X_{g1} + (1-\Upsilon_1)\,, \tag{3.18}$$

$$\begin{aligned}A_2 = {} & 2\left(1-\frac{1}{\chi\mathcal{H}}\right)\frac{\partial b_1}{\partial\ln L} + b_1 f\left[\beta_1 X_{g1} - (1-\Upsilon_1)\right]\\ &+ \left(b_1 f_g + \frac{b_1'}{\mathcal{H}}\right) + b_1\left[1 + b_e - 2\mathcal{Q} - \frac{2\,(1-\mathcal{Q})}{\chi\mathcal{H}} - \frac{\mathcal{H}'}{\mathcal{H}^2}\right]\,,\end{aligned} \tag{3.19}$$

$$\begin{aligned}A_3 = {} & -2(1+\beta_1)X_{g1} + (1+\Upsilon_1) - 2\left[\beta_1 X_{g1} - (1-\Upsilon_1)\right]\\ &- 2 - 2b_e + 4\mathcal{Q} + \frac{4\,(1-\mathcal{Q})}{\chi\mathcal{H}} + 3\frac{\mathcal{H}'}{\mathcal{H}^2}\end{aligned} \tag{3.20}$$

$$A_4 = 1 + (1-\Upsilon_1)^2\,. \tag{3.21}$$

For the standard treatment at second order, we set $\Upsilon_{1,2,} = 0$ and $\beta_{1,2} = 0$. In this limit, we can make use of the Poisson equation to relate the gravitational potential to the matter density

$$X_{g1} = \frac{f_g'}{f_g\mathcal{H}} + f_g + \frac{\mathcal{H}'}{\mathcal{H}^2} = \frac{3}{2}\frac{\Omega_m}{f_g} - 1\,, \tag{3.22}$$

where Ω_m is the matter density parameter, then we recover exactly the result first derived in [35] and discussed in more detail in [21].

3.1 Odd multipoles of the galaxy power spectrum

We obtain the galaxy power spectrum, $P_g^{AB}(k)$, as the expectation value of a two-point correlation function of the galaxy number count of two dissimilar tracers A and B in Fourier space:

$$P_g^{\rm AB}(k,\mu) = \left[\mathcal{K}_{\rm N}^{\rm A}(k,\mu) + i\mathcal{K}_{\rm D}^{\rm A}(k,\mu)\right]\left[\mathcal{K}_{\rm N}^{\rm B}(k,-\mu) + i\mathcal{K}_{\rm D}^{\rm B}(k,-\mu)\right]P_m(z,k)\,. \tag{3.23}$$

Here $P_g^{\rm AB}$ is a complex function and P_m is the matter power spectrum, which is real. In the weak field limit, the real part of $P_g^{\rm AB}$ corresponds to the standard Newtonian approximation or the Kaiser limit, while the imaginary part corresponds to the Doppler part:

JCAP08(2021)049

$P_g^{AB} = P_{g\mathrm{N}}^{AB} + iP_{g\mathrm{D}}^{AB}$ We can isolate the Newtonian and the Doppler parts using

$$P_{g\mathrm{N}}^{AB}(k,\mu) = \frac{1}{2}\left[P_g^{AB}(k,\mu) + P_g^{AB}(k,\mu)^*\right], \tag{3.24}$$

$$P_{g\mathrm{D}}^{AB}(k,\mu) = \frac{1}{2i}\left[P_g^{AB}(k,\mu) - P_g^{AB}(k,\mu)^*\right]. \tag{3.25}$$

The real part is symmetric with respect to the exchange of the line of sight direction: $P_{g\mathrm{N}}^{AB}(k,\mu) = P_{g\mathrm{N}}^{AB}(k,-\mu)$, while the imaginary part is anti-symmetric with respect to the exchange of the line of sight direction: $P_{g\mathrm{D}}^{AB}(k,\mu) = -P_{g\mathrm{D}}^{AB}(k,-\mu)$. Similarly, the real part is symmetric with the exchange of tracer positions: $P_{g\mathrm{N}}^{AB} = P_{g\mathrm{N}}^{BA}$, while the imaginary part is anti-symmetric with the exchange of tracers $P_{g\mathrm{D}}^{AB} = -P_{g\mathrm{D}}^{BA}$. Thus, a simultaneous exchange of tracers and the line of sight direction leaves the imaginary part unchanged.

Tracers with dissimilar astrophysical bias parameters lead to a complex cross-power spectrum and it is possible to expand it using Legendre polynomials, $\mathcal{L}_\ell(\mu)$:

$$P_g^{AB}(z,k,\mu) = \sum_{\ell=0} P_\ell^{AB}(z,k)\mathcal{L}_\ell(\mu)\,. \tag{3.26}$$

The imaginary part of P_g^{AB} induces only the odd multipole moments, which are obtained by using the orthogonality property of the Legendre polynomial

$$P_\ell^{AB}(k) = \frac{(2\ell+1)}{2}\int_{-1}^{1} d\mu\, P^{AB}(k,\mu)\mathcal{L}_\ell(\mu)\,, \tag{3.27}$$

where the multipole moments are given in terms of the matter power spectrum as

$$P_0^{AB}(k) = \left[b_1^A b_1^B + \frac{1}{3}(b_1^A f_g^B + b_1^B f_g^B) + \frac{f_g^A f_g^B}{5}\right] P_m(k)\,, \tag{3.28}$$

$$\begin{aligned} P_1^{AB}(k) = (-i)\Bigg[&\left(b_1^A b_e^B f_g^B - b_1^B b_e^A f_g^A\right) + (b_1^B f_g^A - b_1^A f_g^B)\left[\frac{2}{\chi\mathcal{H}} + \frac{\mathcal{H}'}{\mathcal{H}^2} - \Upsilon_1 - \beta_1 X_{g1}\right] \\ &+ f_g^A f_g^B\left[\frac{3}{5}\left(b_e^B - b_e^A\right) + 3\left(1 - \frac{1}{\chi\mathcal{H}}\right)(s^A - s^B)\right] \\ &+ 5\left(1 - \frac{1}{\chi\mathcal{H}}\right)\left(b_1^B s^A f_g^A - b_1^A s^B f_g^B\right)\Bigg]\frac{\mathcal{H}}{k}P_m(k)\,, \end{aligned} \tag{3.29, 3.30}$$

$$P_2^{AB}(k) = \left[\frac{2}{3}(b_1^A f_g^B + b_1^B f_g^A) + \frac{4 f_g^A f_g^B}{7}\right] P_m(k)\,, \tag{3.31}$$

$$P_3^{AB}(k) = 2i\left[\frac{1}{5}(b_e^A - b_e^B) - \left(1 - \frac{1}{\chi\mathcal{H}}\right)(s^A - s^B)\right] f_g^A f_g^B \frac{\mathcal{H}}{k} P_m(k)\,, \tag{3.32}$$

$$P_4^{AB}(k) = \frac{8}{35} f_g^A f_g^B P_m(k), \tag{3.33}$$

where we have assigned each tracer with a corresponding growth rate for completeness. We note that the baryon-to-dark matter ratio is very similar in different galaxies, therefore we assume it is determined by the cosmological background value as is done in [44], hence, we set $f_g^A = f_g^B = f_g$ in the subsequent quantitive analysis. The odd multipoles vanish in the limit where $A = B$ [45].

JCAP08(2021)049

3.2 Odd multipoles of the galaxy bispectrum

Contrary to the galaxy power spectrum case, the galaxy bispectrum for a single tracer in the weak-field limit is a complex function

$$B_g(z, \boldsymbol{k}_1, \boldsymbol{k}_2, \boldsymbol{k}_3) \equiv B_g^{\rm N}(z, \boldsymbol{k}_1, \boldsymbol{k}_2, \boldsymbol{k}_3) + iB_g^{\rm D}(z, \boldsymbol{k}_1, \boldsymbol{k}_2, \boldsymbol{k}_3)\,, \tag{3.34}$$

where we have identified the real part with the Newtonian limit of the galaxy bispectrum, $B_{\rm N}$; it is given by [46]

$$B_g^{\rm N}(\boldsymbol{k}_1, \boldsymbol{k}_2, \boldsymbol{k}_3) = \mathcal{K}_{\rm N}^{(1)}(\boldsymbol{k}_1)\mathcal{K}_{\rm N}^{(1)}(\boldsymbol{k}_2)\mathcal{K}_{\rm N}^{(2)}(\boldsymbol{k}_1, \boldsymbol{k}_2, \boldsymbol{k}_3)P_m(k_1)P_m(k_2) + 2 \text{ cy. p.} \tag{3.35}$$

The imaginary part corresponds to the galaxy bispectrum induced by the Doppler effects, and its leading contribution is given by [35, 47]

$$\begin{aligned} B_g^{\rm D}(\boldsymbol{k}_1, \boldsymbol{k}_2, \boldsymbol{k}_3) = \Big\{&\mathcal{K}_{\rm N}^{(1)}(\boldsymbol{k}_1)\mathcal{K}_{\rm N}^{(1)}(\boldsymbol{k}_2)\mathcal{K}_{\rm D}^{(2)}(\boldsymbol{k}_1, \boldsymbol{k}_2, \boldsymbol{k}_3) \\ &+ \Big[\mathcal{K}_{\rm N}^{(1)}(\boldsymbol{k}_1)\mathcal{K}_{\rm D}^{(1)}(\boldsymbol{k}_2) + \mathcal{K}_{\rm D}^{(1)}(\boldsymbol{k}_1)\mathcal{K}_{\rm N}^{(1)}(\boldsymbol{k}_2)\Big]\mathcal{K}_{\rm N}^{(2)}(\boldsymbol{k}_1, \boldsymbol{k}_2, \boldsymbol{k}_3)\Big\} \\ &\times P_m(k_1)P_m(k_2) + 2 \text{ cy. p.} \end{aligned} \tag{3.36}$$

Without loss of generality, we work in the plane-parallel limit and express all the three angles in terms of $\mu_1 = \hat{\boldsymbol{k}}_1 \cdot \hat{\mathbf{n}}$. Requiring that $\boldsymbol{k}_1, \boldsymbol{k}_2$ and $\boldsymbol{k}_3$ form a closed triangle, we find

$$\mu_2 = \mu_1\mu_{12} \pm \sqrt{1-\mu_1^2}\sqrt{1-\mu_{12}^2}\cos\phi_n\,, \tag{3.37}$$

$$\mu_3 = -\frac{k_1}{k_3}\mu_1 - \frac{k_2}{k_3}\mu_2\,, \tag{3.38}$$

where $\mu_{12} = \hat{\boldsymbol{k}}_1 \cdot \hat{\boldsymbol{k}}_2$. In this limit, the number of parameters reduces to five, i.e. equations (3.35) and (3.36) depend only on five parameters $B_g(k_1, k_2, \mu_{12}, \mu_1, \phi_n)$. The angular dependence of the galaxy bispectrum relative to the line of sight, i.e μ_1 and ϕ_n may be expanded in spherical harmonics Y_{LM} [46, 48],

$$B_g(k_1, k_2, \mu_{12}, \mu_1, \phi_n) = \sum_{L=0}^{\infty}\sum_{M=-L}^{L} B_{gLM}(k_1, k_2, \mu_{12})Y_L^M(\mu_1, \phi_n), \tag{3.39}$$

where B_{gLM} is the multipole moments of the galaxy bispectrum

$$B_{gLM}(k_1, k_2, \mu_{12}) = \int_{-1}^{1} d\mu_1 \int_0^{2\pi} d\phi_n B_g(k_1, k_2, \mu_{12}, \mu_1, \phi_n)Y_L^{M*}(\mu_1, \phi_n)\,. \tag{3.40}$$

For simplicity, we shall consider only the $M = 0$ moments which reduce to an azimuthal angle averaged galaxy bispectrum or the ϕ_n-average multipole moments of the galaxy bispectrum

$$B_g^{\phi_n}(k_1, k_2, \mu_{12}, \mu_1) \equiv \int_0^{2\pi} B_g(k_1, k_2, \mu_{12}, \mu_1, \phi_n)\frac{d\phi_n}{2\pi}\,. \tag{3.41}$$

Averaging over the azimuthal angles helps to improve the signal to noise ratio [49]. Also, it was shown in [50] that the information loss associated with averaging over the azimuthal angle (or setting $M = 0$) is negligible. We are interested in the multipoles of azimuthal angle averaged galaxy bispectrum, which we compute as

$$B_{gL}(k_1, k_2, \mu_{12}) = \frac{(2L+1)}{2}\int_{-1}^{1} d\mu_1 \int \frac{d\phi_n}{2\pi} B_g(k_1, k_2, \mu_{12}, \mu_1)\mathcal{L}_L(\mu_1). \tag{3.42}$$

JCAP08(2021)049

The even multipoles are sourced by the Newtonian galaxy bispectrum (equation (3.34)) while the odd multipoles are sourced by the Doppler galaxy bispectrum (equation (3.36)). The full multipole decomposition of the relativistic galaxy bispectrum is given in [51].

Finally, we made a plane-parallel approximation to show only the odd multipoles of the cross-power spectrum and the bispectrum that are induced by the general relativistic effects. At the power spectrum level, the wide-angle corrections from the standard density and redshift-space distortion term generate odd multipoles with the same $\mathcal{H}/k$ scale dependence as well. This additional contribution is further suppressed by the ratio of the separation between the sources to the distance to the source. This contribution is obviously sub-dominant in plane-parallel approximation but would become important for a survey that covers the full sky [52]. For the bispectrum, there has not yet been a study of this in detail; however, we expect that the wide-angle corrections from the second-order density and redshift-space distortion terms will lead to a similar conclusion as in the cross-power spectrum case.

4 Fisher forecast analysis of stage IV spectroscopic survey

Our plan is to ascertain how well odd multipole moments of the galaxy cross-power spectrum and bispectrum could constrain the equivalence principle violation through the measurement of these parameters given a stage IV spectroscopic galaxy survey; $\{\Upsilon_1, \Upsilon_2, \beta_1, \beta_2\}$. These parameters are zero if the galaxy motion obeys the equivalence principle, hence any non-zero detection will be an indicator of the violation of the equivalence principle on cosmological scales.

We focus on the late-time violation of the equivalence principle and parametrise $\Upsilon_{1,2}$ as

$$\Upsilon_{1,2}(z) = \frac{1-\Omega_m(z)}{1-\Omega_m}\gamma_{1,2}\,, \tag{4.1}$$

where we have assumed a redshift dependence suggested by [24]. This fixes $\beta_{1,2}$ using equation (2.19), which implies that we are left with only two redshift-independent parameters to describe the violation of the equivalence violation:

$$\text{Equivalence principle violation parameters} = \{\gamma_1, \gamma_2\}\,. \tag{4.2}$$

In order to optimise constraints on these parameters, we fix the following cosmological parameters [10]:

$$\text{Cosmological parameters} = \{D_m, f_g, X_{g1}, X_{g2}, P_{\mathcal{O}}(k)\}\,. \tag{4.3}$$

These parameters will be well constrained by the combination of the Cosmic Microwave Background (CMB) anisotropies and even multipole moments of the power spectrum and bispectrum as well as weak gravitational lensing. Similarly, we assume that the parameters that characterise the Alcock Paczynski effect [53] can be fully determined by the even multipoles of the N-point correlation function [54, 55], hence we neglect these effects in the subsequent analysis. In addition to the cosmological parameters, we have to determine the following astrophysical parameters:

$$\text{Astrophysical parameters} = \left\{b_1, b_2, b_{s^2}, b_e, \mathcal{Q}, \frac{\partial b_1}{\partial \ln \bar{L}}\right\}\,. \tag{4.4}$$

For these parameters we consider a Stage IV Hα emission line galaxy survey and HI intensity mapping survey. We focus on this combination of tracers because an earlier study [45] has shown that the two-point correlation function of the HI intensity mapping and Hα-emission line galaxy spectroscopic galaxy survey leads to a high signal-to-noise ratio (SNR) for detecting the dipole moment.

JCAP08(2021)049

- Hα *emission line galaxies*

  We consider a distribution of the Hα emission line galaxies with a luminosity function [56]

$$\Phi_L(z,L) = \frac{\bar{\Phi}_\star(z)}{\bar{L}_\star(z)} \left(\frac{L}{\bar{L}_\star(z)}\right)^\alpha \exp\left(-\frac{L}{\bar{L}_\star(z)}\right) , \tag{4.5}$$

  where $\bar{L}_\star(z)$ is the critical luminosity at a given redshift and is assumed to evolve as $\bar{L}_\star(z) = \bar{L}_{\star,0}\,(1+z)^2$. Here $L_{\star,0}$ is the critical luminosity today with the best-fit value $\log L_{\star,0} = 41.50$ erg s^{-1}, α is the faint-end slope with the best fit value $\alpha = -1.35$, and $\bar{\Phi}_\star(z)$ is the characteristic number density at z

$$\bar{\Phi}_\star(z) = \begin{cases} \bar{\Phi}_{\star,0}\,(1+z) & \text{for} \quad z < z_{\rm break}\,, \\ \bar{\Phi}_{\star,0}\,(1+z_{\rm break})^2\,/\,(1+z) & \text{for} \quad z > z_{\rm break}\,. \end{cases} \tag{4.6}$$

  $\Phi_{\star,0}$ is the characteristic number density today with the best fit value $\log \bar{\Phi}_{\star,0} = -2.8$ Mpc^{-3} and $z_{\rm break} = 1.3$. The evolution and magnification bias parameters are obtained from equation (4.5) [21]. The number density of the Hα emission line galaxy is obtained from the luminosity function

$$n_g^{\rm H\alpha}(z) = \int_{\ln L} \Phi_L(z,L) d\ln L\,. \tag{4.7}$$

  For the clustering bias parameters we use the values given in [57]

$$b_1^{\rm H\alpha}(z) = 0.9 + 0.4z\,, \tag{4.8}$$
$$b_2^{\rm H\alpha}(z) = -0.704172 - 0.207993z + 0.183023z^2 - 0.00771288z^3\,, \tag{4.9}$$
$$b_{s^2}^{\rm H\alpha}(z) = 0.0321163 - 0.123159z + 0.00694159z^2 - 0.00171397z^3\,. \tag{4.10}$$

  Finally, we set

$$\frac{\partial b_1^{\rm H\alpha}(z,L)}{\partial \ln L} = 0 \tag{4.11}$$

  since $b_1^{\rm H\alpha}(z,L)$ is nearly constant in L [21].

- HI *intensity mapping survey*

  For the HI intensity mapping survey, we follow the prescription given in [58–60] on how to estimate the HI bias parameters from the halo bias parameter. Under this framework, the local HI bias parameters are obtained by assuming that the HI sources are found in galaxies which are resident in halos within a given range of circular velocities. The modelling of this leads to the following HI bias parameters [60];

$$b_1^{\rm HI}(z) = 0.750 + 0.087z + 0.019z^2\,, \tag{4.12}$$
$$b_2^{\rm HI}(z) = -0.257 - 0.063z - 0.007z^2 + 0.006z^3\,, \tag{4.13}$$
$$b_{s^2}^{\rm HI}(z) = -\frac{4}{7}\left(b_1^{\rm HI}(z) - 1\right)\,. \tag{4.14}$$

  The mean HI brightness temperature $\bar{T}$ on the FLRW background is given by [58]

$$\bar{T}_{\rm HI}(z) = \frac{3\pi^2}{4}\frac{\hbar^3 A_{10}}{k_B E_{21}}\frac{\bar{n}_{\rm HI}(z)a(z)^3}{\mathcal{H}(z)} \approx 566h\frac{\Omega_{\rm HI}(z)}{0.003}(1+z)^2\frac{H_0}{\mathcal{H}(z)}\ [\mu{\rm K}], \tag{4.15}$$

JCAP08(2021)049

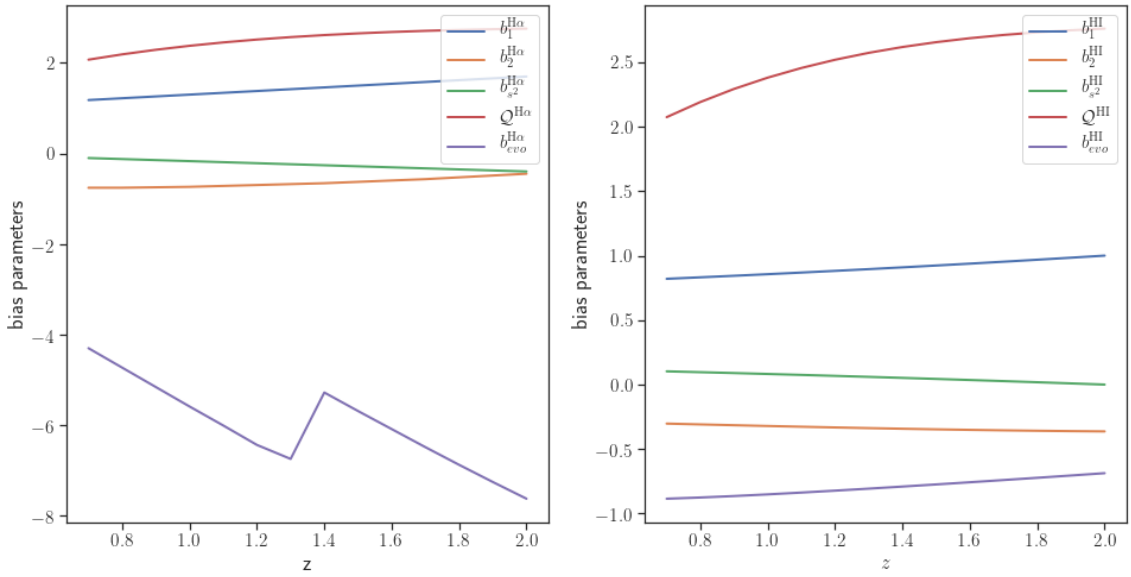

Figure 2. Redshift evolutions of the bias parameters. The left panel shows bias parameters for the H-alpha survey while the right panel shows them for the HI survey. The feature in the H-alpha evolution bias corresponds to the peak of the luminosity function at $z_{\rm break} = 1.3$.

where $\Omega_{\rm HI}$ is the comoving HI mass density. The evolution bias is given by [60]

$$b_{\rm e}^{\rm HI}(z) = -1.248 - 0.147z + 0.145z^2 - 0.012z^3\,. \tag{4.16}$$

HI has a constant magnification bias parameter $\mathcal{Q}^{\rm HI} = 1$ or $s = 2/5$ [61], therefore, $b_1^{\rm HI}$ is constant in luminosity

$$\frac{\partial b_1^{\rm HI}(z, L)}{\partial \ln L} = 0\,. \tag{4.17}$$

Figure 2 shows the redshift evolution of the bias parameters that will be used in the Fisher forecast.

4.1 Estimators of the dipole moment of the galaxy cross-power spectrum

We define the estimator of the dipole moment of the galaxy cross-power spectrum for the dissimilar tracers as the band-power average of the two-point correlation function in Fourier space averaged over all lines of sight and weighted by the angle between $\boldsymbol{k}$ and $\hat{\mathbf{n}}$

$$\overline{P}_{g1}^{AB}(k_i) \equiv \frac{3}{2}\frac{V_s}{V_{12}}\int_{-1}^{1} d\mu\,\mu \int_{\mathcal{K}_i} {\rm d}^3k,\ \Delta_{\rm g}^{\rm A}(\mathbf{k})\,\Delta_{\rm g}^{\rm B}(-\mathbf{k})\,, \tag{4.18}$$

where V_s is the volume of the survey and the estimator is normalised by corresponding volume of the k-bin $\mathcal{K}_i$, $V_{12} \simeq 4\pi k_i^2 \Delta k$. The estimator defined in equation (4.18) for discrete tracers is related to the theory (continuous) galaxy cross-power spectrum according to [62]

$$\langle \Delta_g^A(\boldsymbol{k}_1)\Delta_g^B(\boldsymbol{k}_2)\rangle V_s = \hat{P}_g^{AB}(\boldsymbol{k}_1)\delta^K_{\boldsymbol{k}_1,-\boldsymbol{k}_2} = P_g^{AB}(\boldsymbol{k}_1)\delta^K_{\boldsymbol{k}_1,-\boldsymbol{k}_2} + \frac{\delta^K_{AB}}{\bar{n}_g^A}\delta^K_{\boldsymbol{k}_1,-\boldsymbol{k}_2}\,, \tag{4.19}$$

where δ_{k_1,k_2} is the Kronecker delta and P_g^{AB} is the theory (continuous) cross-power spectrum shown in figure 3.

JCAP08(2021)049

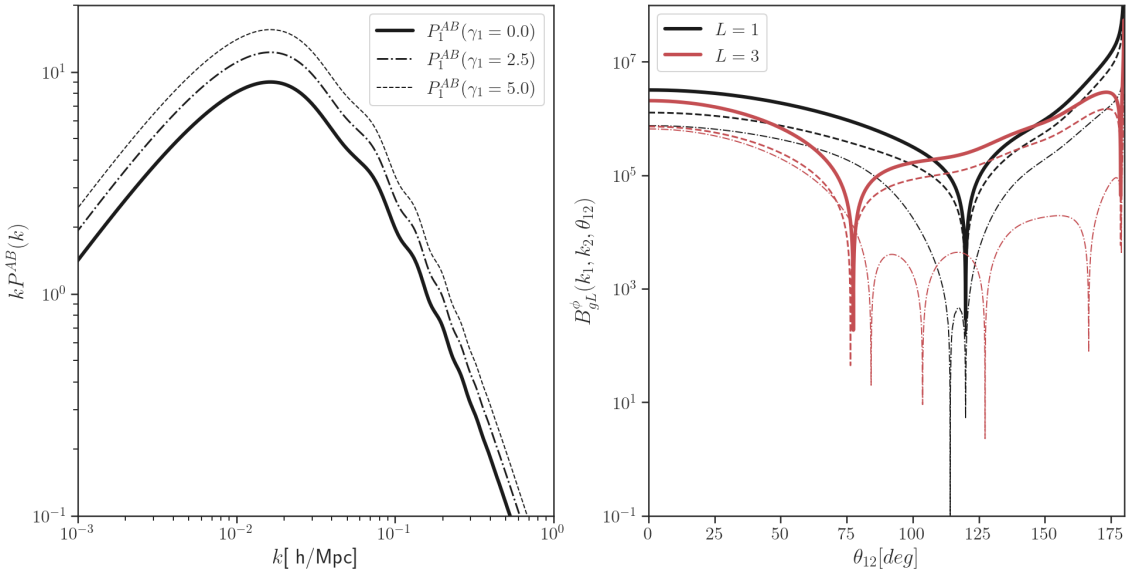

Figure 3. Left panel: the thick line ($\{\gamma_1, \gamma_2\} = \{0, 0\}$) indicates the dipole of the galaxy cross-power spectrum of the Hα emission line galaxy and the HI intensity mapping for a stage IV experiment in the limit of vanishing relative velocity between galaxies and baryons. The dashed ($\{\gamma_1, \gamma_2\} = \{2.5, 2.5\}$) and dashed-dot ($\{\gamma_1, \gamma_2\} = \{5.0, 5.0\}$) lines indicate different amplitude of the relative galaxy-baryon velocity with respect to the galaxy velocity. Right panel: the thick line indicates the bispectrum of the Hα emission line galaxy in the limit of vanishing galaxy-baryon relative velocity. Similarly, the dashed and dashed-dot lines indicate different amplitude of the galaxy-baryon relative velocity with respect to the galaxy velocity just as in the left panel.

In the continuum limit, it becomes

$$\delta^K_{\boldsymbol{k}_1,\boldsymbol{k}'_1} \to \frac{1}{V_s}\delta^D\left(\boldsymbol{k}_1 - \boldsymbol{k}_2\right)(2\pi)^3 = \frac{1}{V_s}\frac{1}{k^2}\delta\left(k - k'\right)\delta\left(\boldsymbol{k}_\perp - \boldsymbol{k}'_\perp\right)(2\pi)^3 . \tag{4.20}$$

To obtain the covariance of the dipole of the cross-power spectrum, we average over the angular k-directions ($\mathrm{d}^3k = k^2 dk d^2\hat{\boldsymbol{k}}$) to obtain an estimator that depends on the wavenumber

$$\begin{aligned}\mathrm{Cov}\left[\overline{P}^{AB}_{g1}(k_i)\overline{P}^{AB}_{g1}(k_j)\right] = \frac{9}{4}\frac{1}{V_{12}}\frac{1}{V'_{12}}\int dk k^2 \int dk' k^2 \int \mathrm{d}^2\boldsymbol{k}\int \mathrm{d}^2\boldsymbol{k}' \\ \times \int d\mu \int d\mu' \mu\mu' \mathrm{Cov}\left[\hat{P}^{AB}_g(\boldsymbol{k})\hat{P}^{AB}_g(\boldsymbol{k}')\right] .\end{aligned} \tag{4.21}$$

The covariant matrix for the galaxy cross-power spectrum is given by [62]

$$\begin{aligned}\mathrm{Cov}\left[\hat{P}^{AB}_g(\boldsymbol{k})\hat{P}^{AB}_g(\boldsymbol{k}')\right] \equiv \frac{(2\pi)^3}{V_s}\Big[\hat{P}^{AA}_g(k,\mu)\hat{P}^{BB}_g(k',-\mu')\delta^D\left(\boldsymbol{k}+\boldsymbol{k}'\right) \\ + \hat{P}^{AB}_g(k,\mu)\hat{P}^{BA}_g(k',-\mu')\delta^D\left(\boldsymbol{k}-\boldsymbol{k}'\right)\Big] .\end{aligned} \tag{4.22}$$

Note that $\hat{P}^{BA}_g(k,-\mu) = \hat{P}^{AB}_g(k,\mu)$ and $P_{BB}(k,-\mu) = P_{BB}(k,\mu)$. We expand the angular dependence of the galaxy power spectrum in Legendre polynomials: $\hat{P}^{AB}_g(k,\mu) = \sum_{L=0}^{4}\hat{P}^{AB}_{gL}(k)\mathcal{L}_L(\mu)$. We find that the multipole moment is given by

$$\hat{P}^{AB}_{gL}(k) = \frac{(2L+1)}{2}\int_{-1}^{1} d\mu\, \hat{P}^{AB}_g(k,\mu)\mathcal{L}_L(\mu) = P^{AB}_{gL}(k) + \delta^K_{AB}\delta_{L0}P^{AA}_{\mathrm{noise}} , \tag{4.23}$$

JCAP08(2021)049

where $P^{AA}_{\rm noise}$ is the noise power spectrum. Expanding $\hat{P}^{BA}_g(k,-\mu)$ in terms of the Legendre polynomial gives

$$\hat{P}^{BA}_g(k,-\mu) = \sum_{L=0}^{4} \hat{P}^{BA}_{gL}(k)\mathcal{L}_L(-\boldsymbol{k}\cdot\hat{\mathbf{n}}) = \sum_{L=0}^{4}(-1)^L\hat{P}^{BA}_{gL}(k)\mathcal{L}_L(\boldsymbol{k}\cdot\hat{\mathbf{n}})\,,$$

where we made use of the parity transformation property of the Legendre polynomial $\mathcal{L}_L(-\boldsymbol{k}\cdot\hat{\mathbf{n}}) = (-1)^L\mathcal{L}_L(\boldsymbol{k}\cdot\hat{\mathbf{n}})$. Note also that $\hat{P}^{BA}_{gL}(k) = (-1)^L\hat{P}^{AB}_{gL}(k)$. Putting all these together leads to

$$\begin{aligned}\mathrm{Cov}\left[\overline{P}^{AB}_{g1}(k_i)\overline{P}^{AB}_{g1}(k_j)\right] = \frac{\delta^K_{k_i,-k'_j}}{N_k}\sum_{L_1L_2}\left[\hat{P}^{AA}_{gL_1}(k_i)\hat{P}^{BB}_{gL_2}(k'_j) - \hat{P}^{AB}_{gL_1}(k_i)\hat{P}^{AB}_{gL_2}(k'_j)\right] \\ \times\int d\mu\mu^2\mathcal{L}_{L_1}(\mu)\;\mathcal{L}_{L_2}(\mu)\,,\end{aligned} \tag{4.24}$$

where we defined $N_k \equiv 4\pi k^2\Delta k V_s/(2\pi)^3$ and made use of the relationship between a 1D Dirac delta function and the Kronecker delta $\delta^D(k+k') \to \delta^K_{k_1,-k'_1}/\Delta k$. The minus sign in the second equality comes from performing the angular integral over the delta function. We perform the integral over μ in equation (4.24) analytically and summed $\{L_1, L_2\}$ up to $\{4, 4\}$ to find

$$\begin{aligned}\mathrm{Cov}\left[\overline{P}^{AB}_{g1}(k_i)\overline{P}^{AB}_{g1}(k_j)\right] = \frac{\delta^K_{k_i,-k'_j}}{N_k}\Bigg\{&\frac{3}{2}\left[P^{AA}_{g0}(k_i)P^{BB}_{\rm noise} + P^{BB}_{g0}(k_j)P^{AA}_{\rm noise} + P^{AA}_{\rm noise}P^{BB}_{\rm noise}\right] \\ &+ \frac{3}{5}\left[P^{AA}_{\rm noise}P^{BB}_{g2}(k_j) + P^{AA}_{g2}(k_i)P^{BB}_{\rm noise}\right] - \frac{9}{10}P^{AB}_{g1}(k_i)P^{AB}_{g1}(k_i) \\ &- \frac{23}{70}P^{AB}_{g3}(k_i)P^{AB}_{g3}(k_i) - \frac{18}{35}P^{AB}_{g3}(k_i)P^{AB}_{g1}(k_i)\Bigg\}\,.\end{aligned} \tag{4.25}$$

Equation (4.25) agrees with [23].

4.2 Estimators of the odd multipoles of the galaxy bispectrum

We define the estimator for the azimuthal angle averaged multipole moments of the galaxy bispectrum following [63] as

$$\begin{aligned}\overline{B}_{g\ell}(k_i,k_j,k_k) \equiv \frac{2\ell+1}{2}\frac{V_{k_f}}{V_{123}}\int_{\mathcal{T}_{i,j}}\mathrm{d}^3k_1\,\mathrm{d}^3k_2\mathrm{d}^3k_3\int\frac{d^2\hat{\mathbf{n}}}{4\pi}\int_0^{2\pi}\frac{d\phi}{2\pi} \\ \times\Delta^{\rm A}_{\rm g}(\boldsymbol{k}_1)\,\Delta^{\rm A}_{\rm g}(\boldsymbol{k}_2)\,\Delta^{\rm A}_{\rm g}(\boldsymbol{k}_3)\delta^{\rm D}\left(\boldsymbol{k}_1+\boldsymbol{k}_2+\boldsymbol{k}_3\right)\mathcal{L}_\ell(\boldsymbol{k}_1\cdot\hat{\mathbf{n}})\,,\end{aligned} \tag{4.26}$$

where $V_k = k_f^3$ is the fundamental k-space cell-volume, k_f is the fundamental wavenumber, which is related to the volume of the survey according to $k_f = 2\pi/L = 2\pi/V_s^{1/3}$, and V_{123} is the effective k-space volume of the k-bin decomposed into spherical shells

$$V_{123} = \int_{\mathcal{T}_i}\delta^{\rm D}(\boldsymbol{p}+\boldsymbol{q}+\boldsymbol{k})\,\mathrm{d}^3p\,\mathrm{d}^3q\,\mathrm{d}^3k \simeq 8\pi^2k_1k_2k_3(\Delta k)^3\beta(\mu_{12})\,. \tag{4.27}$$

Here $\beta(\mu_{12})$ is a normalisation factor that depends on the shape of the triangular configuration [64]

$$\beta(\mu_{12}) = \begin{cases}\frac{1}{2} & \text{if} \quad \mu_{12} = \pm 1 \\ 1 & \text{if} \quad 0 < \mu_{12} < 1 \\ 0 & \text{otherwise}\end{cases} \tag{4.28}$$

JCAP08(2021)049

In the Gaussian limit, the covariance of the galaxy bispectrum becomes [50]

$$\mathrm{Cov}\left[\overline{B}^{A}_{g\ell}\overline{B}^{B}_{g\ell'}\right] \simeq \frac{(2\ell+1)}{2}\frac{(2\ell'+1)}{2}\delta^{K}_{AB}\frac{s_{\rm B}\,V_s}{N_B}\int \mathrm{d}\mu_1 \int \frac{\mathrm{d}\phi}{2\pi}\hat{P}^{AA}_{g}(k_1,\mu_1)\,\hat{P}^{AA}_{g}(k_2,\mu_2)\,\hat{P}^{AA}_{g}(k_3,\mu_3) \times \mathcal{L}_{\ell}(\mu_1)\mathcal{L}_{\ell'}(\mu_1)\,, \tag{4.29}$$

where $s_B = 6, 2, 1$ for equilateral, isosceles and general triangles, respectively and

$$N_B \simeq \frac{1}{\pi}\frac{V^2}{(2\pi)^3}k_1\,k_2\,k_3\,(\Delta k)^3\beta(\mu_{12})\,. \tag{4.30}$$

Each of the power spectrum is decomposed with respect to $\hat{\mathbf{n}}$: $\hat{P}^{AA}_{g}(k_i,\mu_i) = P^{AA}_{g}(k_i,\mu_i) + 1/\bar{n}^{\rm H\alpha}_{g}$. We use equation (3.37) to relate $\{\mu_3,\mu_2\}$ to μ_1 and the azimuthal angle ϕ_n. We performed the integrals over μ_1 and ϕ_n analytically using MATHEMATICA.

4.3 Fisher forecasts for the equivalence principle violation constraint

Firstly, we compute the signal to noise ratio (SNR) for the overlapping HI and Hα spectroscopic surveys using

$$\left(\frac{S}{N}\right)^2 = \sum_{z_{\rm min}}^{z_{\rm max}}\sum_{T_{\rm X}} X_{\ell}(k_i)\mathrm{Cov}^{-1}\left[X_{\ell}(k_i),X_{\ell}(k_j)\right]X^{H}_{\ell}(k_j), \tag{4.31}$$

where X^{H}_{ℓ} is the Hermitian conjugate of $X_\ell = \{P^{AB}_1(k_i), B_1(k_i,k_j,k_k), B_3(k_i,k_j,k_k)\}$, and the summation sign is defined as

$$\sum_{T_{\rm B}} \equiv \sum_{k_1=k_{\rm min}}^{k_{\rm max}}\sum_{k_2=k_1}^{k_{11}}\sum_{k_3=k_\star}^{k_2} \qquad \text{and} \qquad \sum_{T_{\rm P}} = \sum_{k,k'\leq k_{\rm max}} \tag{4.32}$$

for the galaxy bispectrum and cross-power spectrum, respectively. We take the cross-covariances (power spectrum-bispectra and dipole-octupole bispectra covariances) to be zero and set $k_{\rm max}$ at the maximum scale below which the perturbation theory can be trusted: $k_{\rm max} = 0.1(1+z)^{(2/(2+n_s))}[h\mathrm{Mpc}^{-1}]$ [65], $k_{\rm min}$ is determined by the volume of the survey $k_{\rm min} \sim 1/V_s^{1/3}$ and to ensure that the closure property of the triangle is satisfied we have $k_\star = \max(\mathrm{k_{min}}, \mathrm{k_1} - \mathrm{k_2})$. Also, we set the width of the k-bins to $\Delta k = 3k_{\rm min}$. We neglect the covariance between the power spectrum and the bispectrum since we only consider the Gaussian covariance. Also we consider only a single tracer at the bispectrum level. For a single tracer, the odd multipole moment in the power spectrum vanishes. The covariance between the dipole and the octupole of the bispectrum is neglected for simplicity, which is not expected to bias the result since the majority of the signal is contained in the dipole.

The surveys have the following noise attributes; for the Hα emission line galaxy survey, the noise budget is dominated by the shot noise while the HI intensity mapping survey, the noise budget is dominated by the system and sky temperatures

$$P^{\rm H\alpha H\alpha}_{\rm noise} = \frac{1}{n^{\rm H\alpha}_{g}}\,, \qquad P^{\rm HIHI}_{\rm noise} = 4\pi f_{\rm sky}\frac{\chi(z)^2(1+z)^2T_{\rm sys}(z)^2}{N_{\rm pol}N_dH(z)\nu_{21}t_{\rm tot}T^2_{\rm HI}(z)}\,, \tag{4.33}$$

where $N_{\rm pol} = 2$ in equation (4.33) is the polarisation, $t_{\rm tot}$ is the total observing time, N_d is number of dishes and $T_{\rm sys}$ is the sky temperature

$$T_{\rm sys}(z) = 2.7 + 25\left[\frac{400[\mathrm{MHz}](1+\mathrm{z})}{\nu_{21}}\right]^{2.75}\ \mathrm{K}\,, \tag{4.34}$$

where $\nu_{21} = 1420$MHz is the frequency of the 21 cm lime. Table 1 shows the parameters and the redshift range of these surveys.

JCAP08(2021)049

Survey	Redshift range	$f_{\rm sky}$	$t_{\rm tot}$[hrs]	N_d
SKA1-MID Band 1	0.35–3.05	0.48	10000	197
Hα emission line	0.7–2.0	0.35	—	—

Table 1. Survey parameters for the HI intensity mapping survey [66] and Hα emission line survey [16].

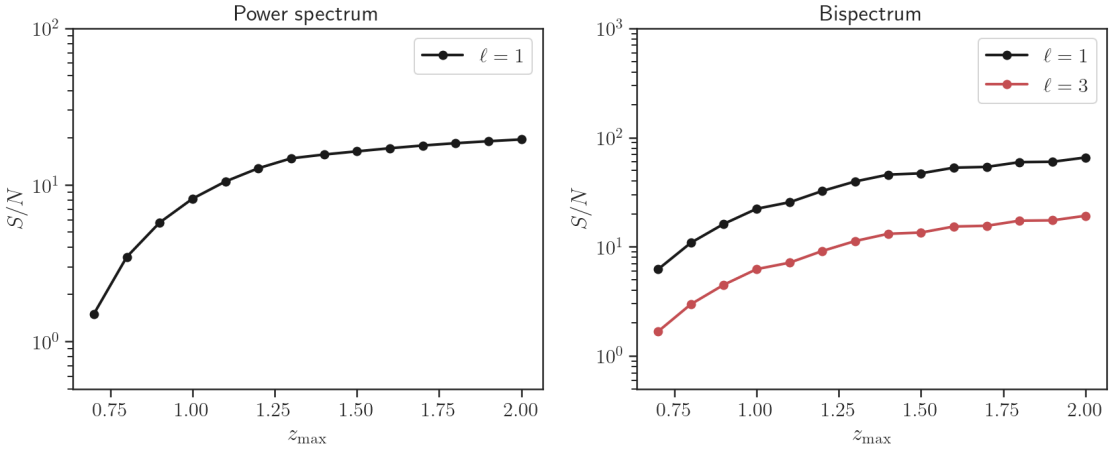

Figure 4. Left panel: this is the SNR for detecting the dipole of the galaxy cross-power spectrum between the Hα line emission galaxy and the HI intensity mapping survey in the single dish mode. Right panel: this is the SNR for detecting the dipole and octupole moments of the Hα bispectrum. We take the fiducial values to be $\{\gamma_1, \gamma_2\} \to \{0, 0\}$.

We neglect the shot noise component of the total noise budget of the HI intensity mapping, as it is usually sub-dominant [58]. Also, we assume that foregrounds have been removed from the HI intensity mapping signal. For recent developments of several foreground removal techniques, see [67]. We show in figure 4 the SNR for detecting the dipole moment of the galaxy cross-power spectrum for the Hα emission line galaxy survey and the HI intensity mapping survey, and the SNR for detecting the dipole and octupole of the Hα galaxy bispectrum. Furthermore, we forecast how well these surveys could constrain the parameters $\{\gamma_1, \gamma_2\}$ using the Fisher information matrix

$$F_{\alpha\beta} = \sum_{z_{\rm min}}^{z_{\rm max}} \sum_{T_{\rm X}} \frac{\partial X_\ell(k_i)}{\partial\theta_\alpha} {\rm Cov}^{-1}\left[X_\ell(k_i), X_\ell(k_j)\right] \frac{\partial X_\ell^H(k_j)}{\partial\theta_\alpha}. \tag{4.35}$$

It measures how steeply the likelihood falls as we move away from the best-fit model. The inverse of the Fisher information matrix approximates the best possible covariance for measurement errors on each parameter θ_α. We calculate parameter constraint (marginal error) using $\sigma_\alpha^2 = \left(F^{-1}\right)_{\alpha\alpha}$. The dipole moment of P_g^{AB} is only sensitive to γ_1 at tree-level, hence we constrain $\theta_\alpha = \{\gamma_1\}$ only. For P_g^{AB}, we assume that the two surveys overlap in about 0.38 fraction of the sky [68], hence our Fisher matrix includes only the overlapping region [69] $F_{\alpha\beta} = F_{\alpha\beta}^{AB}$ (overlap). In principle, this is feasible since the aim of the HI intensity mapping survey is to cover all sky by measuring the intensity of the redshifted 21cm line over the sky without the requirement to resolve individual galaxies [58]. The left panel of figure 5 shows the constraint on γ_1 from P_{AB} as a function of $z_{\rm max}$.

For the galaxy bispectrum we focus only on the Hα emission line galaxy survey to constrain $\theta_\alpha = \{\gamma_1, \gamma_2\}$. We do not use the bispectrum from HI intensity mapping because

JCAP08(2021)049

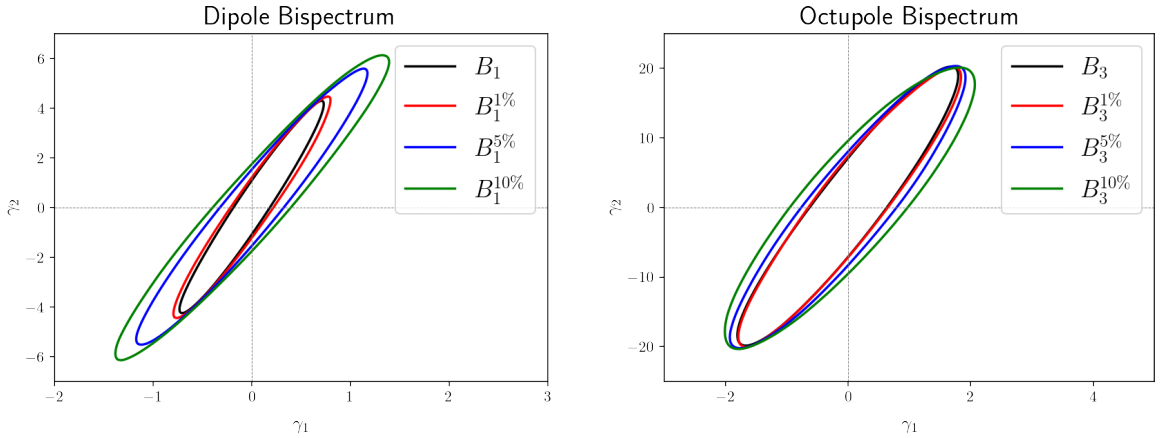

Figure 5. Left panel: 68% confidence ellipse showing the constraint on $\{\gamma_1, \gamma_2\}$ using the dipole of the Hα galaxy bispectrum with various priors on bias parameters. Right panel: just as it is in the left panel but for the octupole moment of the Hα galaxy bispectrum.

of concerns regarding the removal of the very dominant foregrounds; to date, HI intensity mapping has primarily been detected through cross-correlation with the galaxy count [70]. Attempts at finding reliable measurements of the auto-bispectrum of the HI intensity mapping is still in its infancy [71].

Initially we assumed that the bias parameters would be determined precisely by the even multipole moments; however, they will not be determined with perfect accuracy. Therefore, we consider how uncertainties in these parameters will affect the Fisher forecast analysis of the dipole and octupole moment of the Hα galaxy bispectrum. To accomplish this, we parameterise the Hα bias parameters given in equations (4.8) and (4.9) as

$$b_1^{\mathrm{H}\alpha}(z_i) = \mathcal{A}_1 + \mathcal{B}_1 z_i \,, \tag{4.36}$$

$$b_2^{\mathrm{H}\alpha}(z_i) = \mathcal{A}_2 + \mathcal{B}_2 z_i + \mathcal{C}_2 z_i^2 + \mathcal{D}_2 z_i^3 \,, \tag{4.37}$$

where we have introduced the following nuisance parameters

$$\theta_{\mathrm{nuisance}} = \{\mathcal{A}_1, \mathcal{B}_1, \mathcal{A}_2, \mathcal{B}_2, \mathcal{C}_2, \mathcal{D}_2\} \,. \tag{4.38}$$

We assume a local evolution for the tidal field, hence tidal bias parameter becomes $b_{s^2}^{\mathrm{H}\alpha}(z_i) = -4\left(b_1^{\mathrm{H}\alpha}(z_i) - 1\right)/7$ [72]. We adopt the following fiducial values for the nuisance parameters $\theta_{\mathrm{nuisance}}$:

$$\theta_{\mathrm{nuisance}}^{\mathrm{fid}} = \{0.9, 0.4, -0.704172, -0.207992, 0.183023, -0.0007712\} \,. \tag{4.39}$$

These are values are predicted by the halo model given in equations (4.8) and (4.9).

We show in the right panel of figure 5 the 1σ confidence ellipse for $\{\gamma_1, \gamma_2\}$. We considered different Gaussian priors on the nuisance parameters and then marginalised over these; the results are shown in figure 5. We recover the original constraint on $\{\gamma_1, \gamma_2\}$ as long as the nuisance parameters are determined to better than one percent accuracy. This seems achievable from measurements of the even moments [73]. Finally, we show in figure 6 a joint constraint on γ_1 from the combination of the dipole moment of P_{g1}^{AB} and B_{g1}. where we have marginalised over γ_2. Note that with the bispectrum of a single tracer alone we can constrain $\gamma_1 < 0.28$.

JCAP08(2021)049

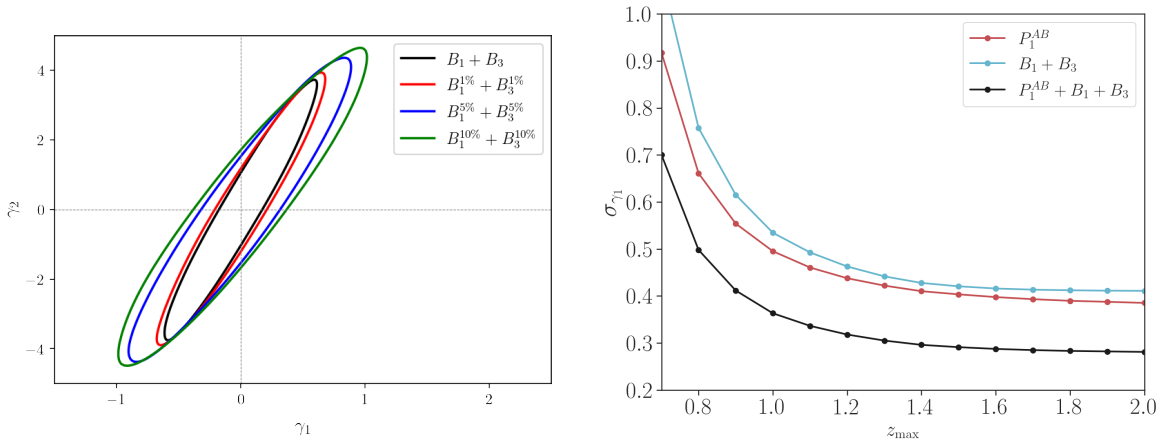

Figure 6. Left panel: 68% confidence ellipse showing the constraint on $\{\gamma_1, \gamma_2\}$ using both dipole and octupole multipole moments of the Hα galaxy bispectrum. Right panel: the joint constraint on γ_1 from the combination of the dipole moment of the galaxy cross-power spectrum and dipole + octupole moments of the Hα galaxy bispectrum, after marginalising over γ_2. We also show the constraint on γ_1 from combined dipole and octupole moments of the bispectrum, after marginalising over γ_2 and the nuisance parameters.

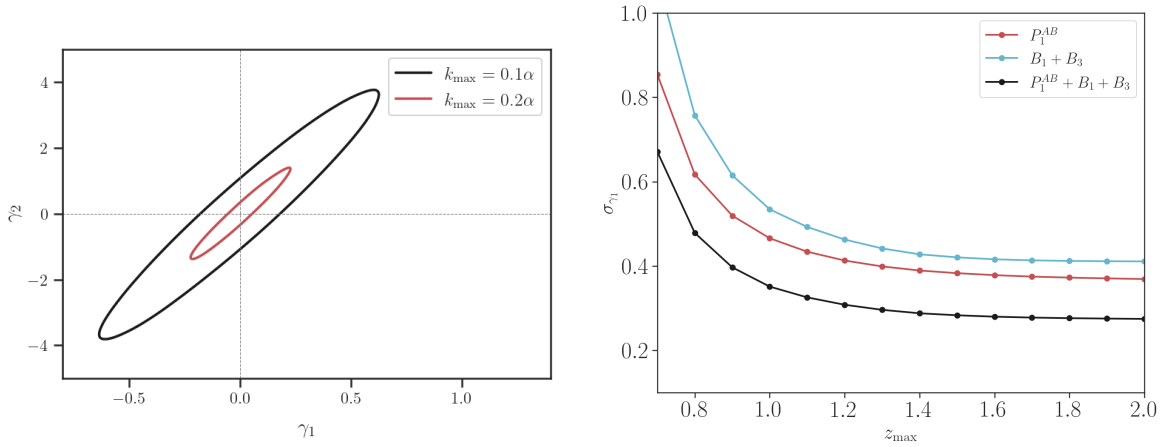

Figure 7. Left panel: 68% confidence ellipse showing the dependence of the constraint on $\{\gamma_1, \gamma_2\}$ using a combination of dipole and octupole for the Hα galaxy bispectrum on $k_{\max}$. Right panel: the joint constraint on γ_1 from the combination of the dipole moment of the galaxy cross-power spectrum and dipole + octupole moments of the Hα galaxy bispectrum with $k_{\max} = 0.2\alpha$. We marginalised over γ_2 and fixed nuisance parameters to their predicted values. Here, $\alpha = (1+z)^{(2/(2+n_s))}[h/\mathrm{Mpc}]$.

The constraint on the galaxy-baryon relative velocity we reported depends sensitively on the choice of $k_{\max}$. We have chosen a very conservative $k_{\max}$ motivated by the range of validity of the cosmological perturbation theory [74]. If, in the future, we are able to improve on the range of modelling accuracy of the fluctuation of the number count of sources to say $k_{\max} = 0.2(1+z)^{(2/(2+n_s))}[h\mathrm{Mpc}^{-1}]$, the constraint on the galaxy-baryon relative velocity could improve significantly. See figure 7. This motivates for further improvement in the modelling of the Doppler contribution to the galaxy cross-power spectrum and bispectrum at higher k including 1-loop corrections [38].

JCAP08(2021)049

5 Conclusion

We have explored in detail how the odd multipoles of the galaxy cross-power spectrum and bispectrum of the number count fluctuations could be used to test the equivalence principle on cosmological scales. We developed this test by relaxing the assumption that the galaxy motion is geodesic (equivalence principle) on all scales in the derivation of the number count fluctuations beyond the Newtonian (Kaiser) approximation. Although the equivalence principle is one of the key principles of general relativity, there is no evidence that it applies to dark matter.

The test we propose assumes that only the types of matter that have been confirmed to obey the equivalence principle at least on solar system scales (e.g. baryons) are geodesic [5]. Our parametrisation assumes the velocity difference between galaxy and baryon is a scale-independent function of the galaxy velocity (equation (2.17)); however, no further assumption was made about the motion of dark matter and the form of interaction in the dark sector. This allowed us to express the violation of the equivalence principle in terms of the galaxy-baryon relative velocity. We parametrise the galaxy-baryon relative velocity in terms of the galaxy velocity, which is measurable. Furthermore, we assume that the joint analysis of the even multipole moments of the galaxy power spectrum and bispectrum will be able to constrain the galaxy velocity, biases and other cosmological parameters to a much higher accuracy, for example see [73][3], leaving the odd multipoles to constrain the equivalence principle.

There are many mechanisms that can generate the relative velocity between baryons and cold dark matter in the Universe. We enumerate a few: (1) Even for purely adiabatic initial perturbations, v_{bc} is induced during baryon-photon decoupling; the tight coupling of baryons to photon forces them to move in a trajectory different from that of the cold dark matter [75]. In this case, it is usually assumed that given sufficient time after decoupling, the baryons will move to trace cold-dark matter but could leave a non-zero v_{bc} at non-linear order [40]. (2) Isocurvature perturbations, potentially generated during inflation in a multi-field scenario, can set an initial condition for v_{bc} [76, 77]. (3) An interaction in the dark sector, such as where cold dark matter is coupled conformally and/or disformally to dark energy; such an interaction will boost v_{bc} at late times. We explore this possibility in greater detail in appendix A.

We have shown that the Stage IV survey could constrain the galaxy-baryon relative velocity to less than 28% of the galaxy velocity using the cross-power spectrum and the bispectrum independently. Our analysis has aimed to be agnostic as to the origin of the galaxy-baryon relative velocity; however our choice of parameterisaton, given by equation (4.1), has implicitly assumed a late time violation of the equivalence principle. To compare to a theory, one would also need to relate the observed galaxy velocities to the velocities of their component parts; in the absence of velocity bias, the galaxy velocity is equal to the matter peculiar velocity v_m, the mass-weighted average of the cold dark matter and baryon velocities [44]: $v_g = v_m = x_{\rm c} v_{\rm c} + x_b v_b$, where $x_{\rm c} = M_{\rm c}/M_g$ and $x_b = M_b/M_g$. Here, $M_{\rm c}$ and M_b are the masses of dark matter and baryon in the galaxy, respectively, and their sum $M_g = M_b + M_{\rm c}$ is the total mass of the galaxy. Therefore, v_{gb} becomes $v_{gb} = x_{\rm c} v_{cb} = -x_{\rm c} v_{bc}$.

[3]The authors show that a cross-correlation analysis of the weak gravitational lensing information and the Hα emission line galaxy clustering information from a Stage IV survey will be able to constrain the linear bias parameter to better than one percent accuracy.

JCAP08(2021)049

Acknowledgments

We would like to thank Florian Beutler and Enea Di Dio for discussions and clarifications on the covariance of the cross-power spectrum. Most of the tensor algebraic computations in this paper were done with the tensor algebra software xPand [78] which is based on xPert [79]. OU, KK and RC are supported by the UK STFC grant ST/S000550/1. KK is also supported by the European Research Council under the European Union's Horizon 2020 programme (grant agreement No.646702 "CosTesGrav").

A The source of baryon-cold dark matter relative velocity

A.1 Interacting dark sector in scalar tensor theory

We discuss how a possible interaction in the dark sector could provide a source for the baryon-dark matter relative velocity and investigate the number of parameters that are required to characterise its evolution. We study a general action for a Scalar-Tensor theory, where the gravitational action is a sum of the action for the quintessence scalar field, S_ϕ, minimally coupled to the Einstein-Hilbert action, $S_{\rm EH}$, in the presence of standard matter, $S_{\rm M}$, and the dark matter field, $S_{\rm c}$,

$$\begin{aligned} S &= \sum_I S_I \\ &= S_{\rm EH}[g_{\mu\nu}] + S_{\rm M}[\text{std matter}, g_{\mu\nu}] + S_\phi[\phi, g_{\mu\nu}] + S_{\rm c}[\text{dark matter}, \tilde{g}_{\mu\nu}]\,, \end{aligned} \tag{A.1}$$

where $S_{\rm c}$ and $S_g = S_{\rm EH} + S_{\rm M} + S_\phi$ are given by [80]

$$S_{\rm c}[\tilde{g}] = \int {\rm d}^4x\sqrt{-\tilde{g}}\,\mathcal{L}_{\rm c}\left(\tilde{g}_{\mu\nu}, \varphi\right)\,, \tag{A.2}$$

$$S_{\rm g}[g] = \int {\rm d}^4x\sqrt{-g}\left[\frac{1}{2\kappa^2}R - \frac{1}{2}g^{\mu\nu}\partial_\mu\phi\partial_\nu\phi - V(\phi) + \mathcal{L}_{\rm M}\right]\,. \tag{A.3}$$

Here φ is a dark matter field, which sees the metric $\tilde{g}_{\mu\nu}$, and $\mathcal{L}_{\rm c}$ is its Lagrangian while $\mathcal{L}_{\rm M}$ is the Lagrangian for the standard matter fields, which instead see the metric $g_{\mu\nu}$. The scalar field ϕ, has a canonical kinetic term with a potential $V(\phi)$ and $\kappa^{-1} \equiv [8\pi G]$ is related to the Planck mass.

We consider a scenario where $\tilde{g}_{\mu\nu}$ is related to $g_{\mu\nu}$ as

$$\tilde{g}_{\mu\nu} = C(\phi)g_{\mu\nu} + D(\phi)\partial_\mu\phi\partial_\nu\phi\,, \tag{A.4}$$

where $C(\phi)$ and $D(\phi)$ are conformal and disformal coupling functions respectively. These functions can also depend on the kinetic term $X = -\partial_\mu\phi\partial_\nu\phi/2$, however, we neglect this dependence going forward for simplicity. In the fluid limit, we can define the energy momentum tensors, $T_I^{\mu\nu}$, associated with each of the fields in equation (A.1) and parameterise each one in terms of the energy density and pressure in its frame of reference according to

$$T_I^{\mu\nu} = \left(\rho_I + P_I\right)u_I^\mu u_I^\nu + P_I g^{\mu\nu}\,. \tag{A.5}$$

Here I indicates the type of matter; $I = {\rm c}$ for the dark matter, $I = \phi$ for the quintessence scalar field and $I = {\rm M}$ standard matter.

JCAP08(2021)049

Each field obeys the following energy-momentum conservation equations

$$\nabla^{\mu} T^{\mathrm{M}}_{\mu\nu} = 0\,, \tag{A.6}$$

$$\nabla^{\mu} T^{\mathrm{c}}_{\mu\nu} = Q\left(\phi, u^{\mu}\nabla_{\mu}\phi, \rho_{\mathrm{c}}\right)\nabla_{\nu}\phi\,. \tag{A.7}$$

The function Q is given by [81]

$$Q\left(\phi, u^{\mu}\nabla_{\mu}\phi, \rho_{\mathrm{c}}\right) = \frac{1}{2}\left\{\frac{d\ln C}{d\phi}T_{\mathrm{c}} + \frac{D}{C}\frac{d\ln D}{d\phi}T^{\mu\nu}_{\mathrm{c}}\nabla_{\mu}\phi\nabla_{\nu}\phi - 2\nabla_{\mu}\left[\frac{D}{C}T^{\mu\nu}_{\mathrm{c}}\nabla_{\nu}\phi\right]\right\}, \tag{A.8}$$

where T_{c} is the trace of the dark matter energy-momentum tensor.

A.2 Interacting dark sector in cosmological perturbation theory

At linear order in cosmological perturbation theory and in the weak field limit, the continuity equations for baryons and dark matter from equations (A.6) and (A.7) are

$$\delta_b^{(1)\prime} = -\partial_i\partial^i v_b^{(1)}\,, \tag{A.9}$$

$$\delta_{\mathrm{c}}^{(1)\prime} = -\partial_i\partial^i v_{\mathrm{c}}^{(1)} - \mathcal{H}\Theta_1\left(1-\Theta_3\right)\delta_{\mathrm{c}}^{(1)}\,, \tag{A.10}$$

and the Euler equations are

$$\partial^i v_b^{(1)\prime} + \mathcal{H}\partial^i v_b^{(1)} + \partial^i\Phi^{(1)} = 0\,, \tag{A.11}$$

$$\partial^i v_{\mathrm{c}}^{(1)\prime} + \mathcal{H}\left[1+\Theta_1\right]\partial^i v_{\mathrm{c}}^{(1)} + \left[1+\Theta_2\right]\partial^i\Phi^{(1)} = 0\,. \tag{A.12}$$

In [24], the authors assumed that $v_g^{(1)} = v_{\mathrm{c}}^{(1)}$, then made use of equation (A.12) to relate the gravitational potential to $v_{\mathrm{c}}^{(1)}$. Here we have introduced the parameterizations following [24]

$$\Theta_1 = -\frac{\bar{\phi}'}{\mathcal{H}}\frac{\bar{Q}}{\bar{\rho}_{\mathrm{c}}}\,, \qquad \Theta_2 = -\frac{\bar{Q}^2}{\kappa\bar{\rho}_{\mathrm{c}}} \qquad \Theta_3 = \frac{\partial\ln\bar{Q}}{\partial\ln\rho_{\mathrm{c}}}\,. \tag{A.13}$$

These parameters parametrise the violation of the equivalence principle due to the fact that dark matter moves in a geodesic that is different from that of the standard matter because of the interaction with the quintessence scalar field through the conformal or the disformal coupling. This shows that we need three free parameters to describe the evolution of the dark matter density and velocity at linear order.

Similarly at the second order, the continuity equations for baryons and dark matter are given by

$$\delta_b^{(2)\prime} = -\partial_i\partial^i v_b^{(2)} + 2\delta_b^{(1)}\partial_i\partial^i v_b^{(1)} + 2\partial_i v_b^{(1)}\partial^i\delta_b^{(1)} + \mathcal{O}\left((\partial\Phi^{(1)})^2\right)\,, \tag{A.14}$$

$$\begin{aligned}\delta_{\mathrm{c}}^{(2)\prime} = &-\partial_i\partial^i v_{\mathrm{c}}^{(2)} - \mathcal{H}\left[\Theta_1\left(1-\Theta_3\right)\delta_{\mathrm{c}}^{(2)}\right] + 2\delta_{\mathrm{c}}^{(1)}\partial_i\partial^i v_{\mathrm{c}}^{(1)} + 2\partial_i v_{\mathrm{c}}^{(1)}\partial^i\delta_{\mathrm{c}}^{(1)} \\ &+ \Theta_1\Theta_4(\delta_{\mathrm{c}}^{(1)})^2 + \mathcal{O}\left((\partial\Phi^{(1)})^2\right)\,.\end{aligned} \tag{A.15}$$

The corresponding Euler equation become

$$\partial_i v_b^{(2)\prime} + \mathcal{H}\partial_i v_b^{(2)} + \partial_i\Phi^{(2)} + 2\partial_i\partial_j v_b^{(1)}\partial^j v_b^{(1)} + \mathcal{O}(\Phi^{(1)}\partial\Phi) = 0\,, \tag{A.16}$$

$$\begin{aligned}\partial_i v_{\mathrm{c}}^{(2)\prime} &+ \mathcal{H}\left[1+\Theta_1\right]\partial_i v_{\mathrm{c}}^{(2)} + \left[1+\Theta_2\right]\partial_i\Phi^{(2)} + 2\partial_i\partial_j v^{(1)}\partial^j v^{(1)} \\ &+ 2\mathcal{H}\Theta_1\left(\Theta_3-1\right)\delta_{\mathrm{c}}^{(1)}\partial_i v_{\mathrm{c}}^{(1)} - 2\Theta_2\left(1-\Theta_3\right)\delta_{\mathrm{c}}^{(1)}\partial_i\Phi^{(1)} + \mathcal{O}(\Phi^{(1)}\partial\Phi) = 0\,,\end{aligned} \tag{A.17}$$

JCAP08(2021)049

where we have introduced yet another parameter to describe the self-coupling strength of the dark matter density field

$$\Theta_4 = \frac{1}{Q}\frac{\partial^2 Q}{(\partial \ln \rho_c)^2} \,. \tag{A.18}$$

The second order dark matter density and velocity can be obtained by solving these equations. Note that, since the gravitational potential is sourced by the dark matter and baryon density, the equations for baryons and cold dark matter are coupled.

We have shown that we need four free parameters $\{\Theta_1, \Theta_2, \Theta_3, \Theta_4\}$ in order to characterise the interaction between dark matter and baryons in this model. By specifying these parameters, we can compute the relative velocity between baryons and dark matter, and predict the equivalence principle violation parameters $\Upsilon_{1,2}$ and $\beta_{1,2}$.

References

[1] K. Koyama, *Cosmological Tests of Modified Gravity*, *Rept. Prog. Phys.* **79** (2016) 046902 [arXiv:1504.04623] [INSPIRE].

[2] C. van de Bruck, J. Mifsud, J.P. Mimoso and N.J. Nunes, *Generalized dark energy interactions with multiple fluids*, *JCAP* **11** (2016) 031 [arXiv:1605.03834] [INSPIRE].

[3] C.C. Speake and C.M. Will, *Tests of the weak equivalence principle*, *Class. Quant. Grav.* **29** (2012) 180301.

[4] L. Zhou et al., *United test of the equivalence principle at* 10^{-10} *level using mass and internal energy specified atoms*, arXiv:1904.07096 [INSPIRE].

[5] P. Touboul et al., *MICROSCOPE Mission: First Results of a Space Test of the Equivalence Principle*, *Phys. Rev. Lett.* **119** (2017) 231101 [arXiv:1712.01176] [INSPIRE].

[6] J.-J. Wei, H. Gao, X.-F. Wu and P. Mészáros, *Testing Einstein's Equivalence Principle With Fast Radio Bursts*, *Phys. Rev. Lett.* **115** (2015) 261101 [arXiv:1512.07670] [INSPIRE].

[7] L. Giani and E. Frion, *Testing the Equivalence Principle with Strong Lensing Time Delay Variations*, *JCAP* **09** (2020) 008 [arXiv:2005.07533] [INSPIRE].

[8] S.-C. Yang, W.-B. Han and G. Wang, *Tests of weak equivalence principle with the gravitational wave signals in the LIGO-Virgo catalogue GWTC-1*, *Mon. Not. Roy. Astron. Soc.* **499** (2020) L53 [arXiv:1912.10758] [INSPIRE].

[9] C.W. Stubbs, *Experimental limits on any long range nongravitational interaction between dark matter and ordinary matter*, *Phys. Rev. Lett.* **70** (1993) 119 [INSPIRE].

[10] Planck collaboration, *Planck 2018 results. VI. Cosmological parameters*, *Astron. Astrophys.* **641** (2020) A6 [*Erratum ibid.* **652** (2021) C4] [arXiv:1807.06209] [INSPIRE].

[11] C. Clarkson, G. Ellis, J. Larena and O. Umeh, *Does the growth of structure affect our dynamical models of the universe? The averaging, backreaction and fitting problems in cosmology*, *Rept. Prog. Phys.* **74** (2011) 112901 [arXiv:1109.2314] [INSPIRE].

[12] C. Clarkson and O. Umeh, *Is backreaction really small within concordance cosmology?*, *Class. Quant. Grav.* **28** (2011) 164010 [arXiv:1105.1886] [INSPIRE].

[13] P. Creminelli, J. Gleyzes, L. Hui, M. Simonović and F. Vernizzi, *Single-Field Consistency Relations of Large Scale Structure. Part III: Test of the Equivalence Principle*, *JCAP* **06** (2014) 009 [arXiv:1312.6074] [INSPIRE].

[14] A. Kehagias, J. Noreña, H. Perrier and A. Riotto, *Consequences of Symmetries and Consistency Relations in the Large-Scale Structure of the Universe for Non-local bias and Modified Gravity*, *Nucl. Phys. B* **883** (2014) 83 [arXiv:1311.0786] [INSPIRE].

JCAP08(2021)049

[15] N. Kaiser, *Clustering in real space and in redshift space*, *Mon. Not. Roy. Astron. Soc.* **227** (1987) 1 [INSPIRE].

[16] L. Amendola et al., *Cosmology and fundamental physics with the Euclid satellite*, *Living Rev. Rel.* **21** (2018) 2 [arXiv:1606.00180] [INSPIRE].

[17] D.J. Bacon, S. Andrianomena, C. Clarkson, K. Bolejko and R. Maartens, *Cosmology with Doppler Lensing*, *Mon. Not. Roy. Astron. Soc.* **443** (2014) 1900 [arXiv:1401.3694] [INSPIRE].

[18] C. Bonvin, L. Hui and E. Gaztanaga, *Optimising the measurement of relativistic distortions in large-scale structure*, *JCAP* **08** (2016) 021 [arXiv:1512.03566] [INSPIRE].

[19] C. Bonvin et al., *Dipolar modulation in the size of galaxies: The effect of Doppler magnification*, *Mon. Not. Roy. Astron. Soc.* **472** (2017) 3936 [arXiv:1610.05946] [INSPIRE].

[20] E. Di Dio and U. Seljak, *The relativistic dipole and gravitational redshift on LSS*, *JCAP* **04** (2019) 050 [arXiv:1811.03054] [INSPIRE].

[21] R. Maartens, S. Jolicoeur, O. Umeh, E.M. De Weerd, C. Clarkson and S. Camera, *Detecting the relativistic galaxy bispectrum*, *JCAP* **03** (2020) 065 [arXiv:1911.02398] [INSPIRE].

[22] E. Gaztanaga, C. Bonvin and L. Hui, *Measurement of the dipole in the cross-correlation function of galaxies*, *JCAP* **01** (2017) 032 [arXiv:1512.03918] [INSPIRE].

[23] F. Beutler and E. Di Dio, *Modeling relativistic contributions to the halo power spectrum dipole*, *JCAP* **07** (2020) 048 [arXiv:2004.08014] [INSPIRE].

[24] C. Bonvin and P. Fleury, *Testing the equivalence principle on cosmological scales*, *JCAP* **05** (2018) 061 [arXiv:1803.02771] [INSPIRE].

[25] G.F.R. Ellis, *Republication of: Relativistic cosmology*, *Gen. Rel. Grav.* **41** (2009) 581 [INSPIRE].

[26] A. Challinor and A. Lewis, *The linear power spectrum of observed source number counts*, *Phys. Rev. D* **84** (2011) 043516 [arXiv:1105.5292] [INSPIRE].

[27] D. Alonso, P. Bull, P.G. Ferreira, R. Maartens and M. Santos, *Ultra large-scale cosmology in next-generation experiments with single tracers*, *Astrophys. J.* **814** (2015) 145 [arXiv:1505.07596] [INSPIRE].

[28] D. Bertacca, *Observed galaxy number counts on the light cone up to second order: III. Magnification bias*, *Class. Quant. Grav.* **32** (2015) 195011 [arXiv:1409.2024] [INSPIRE].

[29] E. Di Dio, R. Durrer, G. Marozzi and F. Montanari, *The bispectrum of relativistic galaxy number counts*, *JCAP* **01** (2016) 016 [arXiv:1510.04202] [INSPIRE].

[30] J. Yoo and M. Zaldarriaga, *Beyond the Linear-Order Relativistic Effect in Galaxy Clustering: Second-Order Gauge-Invariant Formalism*, *Phys. Rev. D* **90** (2014) 023513 [arXiv:1406.4140] [INSPIRE].

[31] S. Jolicoeur, A. Allahyari, C. Clarkson, J. Larena, O. Umeh and R. Maartens, *Imprints of local lightcone projection effects on the galaxy bispectrum IV: second-order vector and tensor contributions*, *JCAP* **03** (2019) 004 [arXiv:1811.05458] [INSPIRE].

[32] F. Montanari and R. Durrer, *Measuring the lensing potential with tomographic galaxy number counts*, *JCAP* **10** (2015) 070 [arXiv:1506.01369] [INSPIRE].

[33] G. Jelic-Cizmek, F. Lepori, C. Bonvin and R. Durrer, *On the importance of lensing for galaxy clustering in photometric and spectroscopic surveys*, *JCAP* **04** (2021) 055 [arXiv:2004.12981] [INSPIRE].

[34] O. Umeh, C. Clarkson and R. Maartens, *Nonlinear relativistic corrections to cosmological distances, redshift and gravitational lensing magnification. II — Derivation*, *Class. Quant. Grav.* **31** (2014) 205001 [arXiv:1402.1933] [INSPIRE].

JCAP08(2021)049

[35] C. Clarkson, E.M. de Weerd, S. Jolicoeur, R. Maartens and O. Umeh, *The dipole of the galaxy bispectrum*, *Mon. Not. Roy. Astron. Soc.* **486** (2019) L101 [arXiv:1812.09512] [INSPIRE].

[36] C. Bonvin and R. Durrer, *What galaxy surveys really measure*, *Phys. Rev. D* **84** (2011) 063505 [arXiv:1105.5280] [INSPIRE].

[37] J. Yoo, *General Relativistic Description of the Observed Galaxy Power Spectrum: Do We Understand What We Measure?*, *Phys. Rev. D* **82** (2010) 083508 [arXiv:1009.3021] [INSPIRE].

[38] E. Di Dio and F. Beutler, *The relativistic galaxy number counts in the weak field approximation*, *JCAP* **09** (2020) 058 [arXiv:2004.07916] [INSPIRE].

[39] D. Tseliakhovich and C. Hirata, *Relative velocity of dark matter and baryonic fluids and the formation of the first structures*, *Phys. Rev. D* **82** (2010) 083520 [arXiv:1005.2416] [INSPIRE].

[40] A. Barreira, G. Cabass, D. Nelson and F. Schmidt, *Baryon-CDM isocurvature galaxy bias with IllustrisTNG*, *JCAP* **02** (2020) 005 [arXiv:1907.04317] [INSPIRE].

[41] F. Schmidt, *Effect of relative velocity and density perturbations between baryons and dark matter on the clustering of galaxies*, *Phys. Rev. D* **94** (2016) 063508 [arXiv:1602.09059] [INSPIRE].

[42] O. Umeh, K. Koyama, R. Maartens, F. Schmidt and C. Clarkson, *General relativistic effects in the galaxy bias at second order*, *JCAP* **05** (2019) 020 [arXiv:1901.07460] [INSPIRE].

[43] F. Bernardeau, S. Colombi, E. Gaztanaga and R. Scoccimarro, *Large scale structure of the universe and cosmological perturbation theory*, *Phys. Rept.* **367** (2002) 1 [astro-ph/0112551] [INSPIRE].

[44] J. Gleyzes, D. Langlois, M. Mancarella and F. Vernizzi, *Effective Theory of Dark Energy at Redshift Survey Scales*, *JCAP* **02** (2016) 056 [arXiv:1509.02191] [INSPIRE].

[45] A. Hall and C. Bonvin, *Measuring cosmic velocities with 21 cm intensity mapping and galaxy redshift survey cross-correlation dipoles*, *Phys. Rev. D* **95** (2017) 043530 [arXiv:1609.09252] [INSPIRE].

[46] R. Scoccimarro, H.M.P. Couchman and J.A. Frieman, *The Bispectrum as a Signature of Gravitational Instability in Redshift-Space*, *Astrophys. J.* **517** (1999) 531 [astro-ph/9808305] [INSPIRE].

[47] O. Umeh, S. Jolicoeur, R. Maartens and C. Clarkson, *A general relativistic signature in the galaxy bispectrum: the local effects of observing on the lightcone*, *JCAP* **03** (2017) 034 [arXiv:1610.03351] [INSPIRE].

[48] R. Scoccimarro, *The bispectrum: from theory to observations*, *Astrophys. J.* **544** (2000) 597 [astro-ph/0004086] [INSPIRE].

[49] N. Bartolo, E. Komatsu, S. Matarrese and A. Riotto, *Non-Gaussianity from inflation: Theory and observations*, *Phys. Rept.* **402** (2004) 103 [astro-ph/0406398] [INSPIRE].

[50] P. Gagrani and L. Samushia, *Information Content of the Angular Multipoles of Redshift-Space Galaxy Bispectrum*, *Mon. Not. Roy. Astron. Soc.* **467** (2017) 928 [arXiv:1610.03488] [INSPIRE].

[51] E.M. de Weerd, C. Clarkson, S. Jolicoeur, R. Maartens and O. Umeh, *Multipoles of the relativistic galaxy bispectrum*, *JCAP* **05** (2020) 018 [arXiv:1912.11016] [INSPIRE].

[52] C. Bonvin, L. Hui and E. Gaztanaga, *Asymmetric galaxy correlation functions*, *Phys. Rev. D* **89** (2014) 083535 [arXiv:1309.1321] [INSPIRE].

[53] C. Alcock and B. Paczynski, *An evolution free test for non-zero cosmological constant*, *Nature* **281** (1979) 358 [INSPIRE].

JCAP08(2021)049

[54] S. Nadathur, P.M. Carter, W.J. Percival, H.A. Winther and J. Bautista, *Beyond BAO: Improving cosmological constraints from BOSS data with measurement of the void-galaxy cross-correlation*, *Phys. Rev. D* **100** (2019) 023504 [arXiv:1904.01030] [INSPIRE].

[55] A. de Mattia et al., *The Completed SDSS-IV extended Baryon Oscillation Spectroscopic Survey: measurement of the BAO and growth rate of structure of the emission line galaxy sample from the anisotropic power spectrum between redshift 0.6 and 1.1*, *Mon. Not. Roy. Astron. Soc.* **501** (2021) 5616 [arXiv:2007.09008] [INSPIRE].

[56] L. Pozzetti et al., *Modelling the number density of Hα emitters for future spectroscopic near-IR space missions*, *Astron. Astrophys.* **590** (2016) A3 [arXiv:1603.01453] [INSPIRE].

[57] V. Yankelevich and C. Porciani, *Cosmological information in the redshift-space bispectrum*, *Mon. Not. Roy. Astron. Soc.* **483** (2019) 2078 [arXiv:1807.07076] [INSPIRE].

[58] M.G. Santos et al., *Cosmology from a SKA HI intensity mapping survey*, *PoS* **AASKA14** (2015) 019 [arXiv:1501.03989] [INSPIRE].

[59] O. Umeh, R. Maartens and M. Santos, *Nonlinear modulation of the HI power spectrum on ultra-large scales. I*, *JCAP* **03** (2016) 061 [arXiv:1509.03786] [INSPIRE].

[60] O. Umeh, *Imprint of non-linear effects on HI intensity mapping on large scales*, *JCAP* **06** (2017) 005 [arXiv:1611.04963] [INSPIRE].

[61] E. Di Dio et al., *Non-Gaussianities due to Relativistic Corrections to the Observed Galaxy Bispectrum*, *JCAP* **03** (2017) 006 [arXiv:1611.03720] [INSPIRE].

[62] R.E. Smith, *Covariance of cross-correlations: towards efficient measures for large-scale structure*, *Mon. Not. Roy. Astron. Soc.* **400** (2009) 851 [arXiv:0810.1960] [INSPIRE].

[63] D. Regan, *An Inventory of Bispectrum Estimators for Redshift Space Distortions*, *JCAP* **12** (2017) 020 [arXiv:1708.05303] [INSPIRE].

[64] K.C. Chan and L. Blot, *Assessment of the Information Content of the Power Spectrum and Bispectrum*, *Phys. Rev. D* **96** (2017) 023528 [arXiv:1610.06585] [INSPIRE].

[65] EUCLID collaboration, *Euclid preparation: VII. Forecast validation for Euclid cosmological probes*, *Astron. Astrophys.* **642** (2020) A191 [arXiv:1910.09273] [INSPIRE].

[66] Z. Ahmed et al., *Research and Development for HI Intensity Mapping*, arXiv:1907.13090 [INSPIRE].

[67] S. Cunnington, L. Wolz, A. Pourtsidou and D. Bacon, *Impact of foregrounds on HI intensity mapping cross-correlations with optical surveys*, *Mon. Not. Roy. Astron. Soc.* **488** (2019) 5452 [arXiv:1904.01479] [INSPIRE].

[68] J. Fonseca, S. Camera, M. Santos and R. Maartens, *Hunting down horizon-scale effects with multi-wavelength surveys*, *Astrophys. J. Lett.* **812** (2015) L22 [arXiv:1507.04605] [INSPIRE].

[69] J.-A. Viljoen, J. Fonseca and R. Maartens, *Constraining the growth rate by combining multiple future surveys*, *JCAP* **09** (2020) 054 [arXiv:2007.04656] [INSPIRE].

[70] K.W. Masui et al., *Measurement of 21 cm brightness fluctuations at $z \sim 0.8$ in cross-correlation*, *Astrophys. J. Lett.* **763** (2013) L20 [arXiv:1208.0331] [INSPIRE].

[71] S. Jolicoeur, R. Maartens, E.M. De Weerd, O. Umeh, C. Clarkson and S. Camera, *Detecting the relativistic bispectrum in 21cm intensity maps*, *JCAP* **06** (2021) 039 [arXiv:2009.06197] [INSPIRE].

[72] V. Desjacques, D. Jeong and F. Schmidt, *Large-Scale Galaxy Bias*, *Phys. Rept.* **733** (2018) 1 [arXiv:1611.09787] [INSPIRE].

[73] EUCLID collaboration, *Euclid: The importance of galaxy clustering and weak lensing cross-correlations within the photometric Euclid survey*, *Astron. Astrophys.* **643** (2020) A70 [arXiv:2005.00055] [INSPIRE].

JCAP08(2021)049

[74] R.E. Smith, R.K. Sheth and R. Scoccimarro, *An analytic model for the bispectrum of galaxies in redshift space*, *Phys. Rev. D* **78** (2008) 023523 [arXiv:0712.0017] [INSPIRE].

[75] C. Pitrou, *The tight-coupling approximation for baryon acoustic oscillations*, *Phys. Lett. B* **698** (2011) 1 [arXiv:1012.0546] [INSPIRE].

[76] K.A. Malik and D. Wands, *Adiabatic and entropy perturbations with interacting fluids and fields*, *JCAP* **02** (2005) 007 [astro-ph/0411703] [INSPIRE].

[77] P. Carrilho and K.A. Malik, *Isocurvature initial conditions for second order Boltzmann solvers*, *JCAP* **08** (2018) 020 [arXiv:1803.08939] [INSPIRE].

[78] C. Pitrou, X. Roy and O. Umeh, *xPand: An algorithm for perturbing homogeneous cosmologies*, *Class. Quant. Grav.* **30** (2013) 165002 [arXiv:1302.6174] [INSPIRE].

[79] D. Brizuela, J.M. Martin-Garcia and G.A. Mena Marugan, *xPert: Computer algebra for metric perturbation theory*, *Gen. Rel. Grav.* **41** (2009) 2415 [arXiv:0807.0824] [INSPIRE].

[80] C. Van De Bruck and J. Mifsud, *Searching for dark matter-dark energy interactions: going beyond the conformal case*, *Phys. Rev. D* **97** (2018) 023506 [arXiv:1709.04882] [INSPIRE].

[81] J. Mifsud and C. Van De Bruck, *Probing the imprints of generalized interacting dark energy on the growth of perturbations*, *JCAP* **11** (2017) 001 [arXiv:1707.07667] [INSPIRE].

JCAP08(2021)049